Faculty of Postgraduate Studies and Scientific Research

German University in Cairo

Wireless Control of Magnetic Drug Carriers using a Magnetic-Based Robotic System

A thesis submitted in partial fulfillment of the requirements for the degree of Master of Science in Mechatronics Engineering

By

Bishoy Emil Edward Wissa

Supervised by

Dr. Islam S. M. Khalil

Prof. Dr. E. I. Imam Morgan

June, 2015

Declaration of Authorship

I, Bishoy Emil, declare that this thesis titled, 'Thesis Title' and the work presented in it are my own. I confirm that:

- This work was done wholly or mainly while in candidature for a research degree at this University.
- Where any part of this thesis has previously been submitted for a degree or any other qualification at this University or any other institution, this has been clearly stated.
- Where I have consulted the published work of others, this is always clearly attributed.
- Where I have quoted from the work of others, the source is always given. With the exception of such quotations, this thesis is entirely my own work.
- I have acknowledged all main sources of help.
- Where the thesis is based on work done by myself jointly with others, I have made clear exactly what was done by others and what I have contributed myself.

Signed:

Date:

Contents

List of Figures

List of Tables

Acknowledgements

It is a great pleasure to express my profound gratitude and sincere appreciation to Dr. Islam S. M. Khalil for the planning of this work and for his constant supervision with a continuous enthusiastic encouragement. I have benefited so much from his guidelines and discussions to the details on my research and he has willing to make time for me no matter how busy he was.

In addition, I would like to express my gratitude to Prof. Dr. Imam Morgan for his support and continuous encouragement. Also I want to thank him for his precious advices. He always treats me like his own son.

Special thanks to Eng. Omar Mahmoud who always stepped forward to help me during the progress of this work.

I will always be thankful to my parents Eng. Emil Edward and Assoc. Prof. Dr. Eng. Eman Tharwat at the Egyptian Nuclear and Radiological Regulatory Authority and my sister Marina for creating the best environment for me to learn, their unceasing encouragement, their support and their love that carried me through the rough times of life.

Abstract

The side-effects of many drugs can be mitigated by using targeted drug delivery. The drug is localized within the vicinity of the small location of the disease inside the human body. In this thesis, motion control of paramagnetic microparticles is achieved using a magnetic-based robotic system with an open-configuration. This control is done using a permanent magnet and an electromagnetic coil under microscopic guidance and using visual feedback. The permanent magnet and the electromagnetic coils are fixed to the end-effector of a robotic arm with 4 degrees-of-freedom to control the position of the microparticles. A closed-loop motion control of the robotic arm is done at the joint-space to orient the magnetic field gradients of the permanent magnet and the electromagnetic coil towards a reference point. Point-to-point motion control is achieved at an average speed of 117 μm/s using the permanent magnet and the robotic arm, whereas the electromagnetic coil and the robotic arm achieve average speed of 48 μm/s. In addition, the permanent magnet and the robotic arm achieve maximum position error of 600 μm, in the steady-state, as opposed to 100 μm for the electromagnetic coil and the robotic arm using P controller. The precise motion control of paramagnetic microparticles using a magnetic system with open-configuration provides broad possibilities in targeted therapy and biomedical applications that cannot be achieved using magnetic systems with closed-configurations.

Chapter 1

Introduction and Background

1.1 Introduction

Robots can exist nowadays in two different scales: macroscale and microscale. Macroscale robots shown in Fig. 1.1 are more common and they are two types: industrial robots (e.g., robotic arms used in material handling, material transfer, machine loading or unloading, assembly, inspection, surgeries as da vinci robot and etc) and mobile robots (e.g, humanoid robots, unmanned arial vehicles (UAV), demining robots, climbing robots, military robots and etc).

1.1.1 Importance of Microscale robots

In spite of all these applications of macroscale robots, their size makes them unable to access very small places whose size do not exceed a few millimeters. The need to reach microscale places necessitates the development of robots in

the microscale. The size of microrobots (only a few millimeters or less) provides them with a very important and vital role in many critical fields (e.g, targeted therapy [1], material removal [2], controllable structures [3] and telemetry [2]).

The fundamental physics that governs the macroscale robots and microscale robots remains the same but the relative importance of physical effects changes as scaling robots to the microscale. In marcoscale robots, physical effects as fluid viscosity and surface effects such as electrostatics dominate over volumetric effects such as weight and inertia which affects macroscale robots. In addition to this, power generation and storage becomes difficult in case of microscale robots which places strong constraints on the development of these robots. The design of macroscale robots focuses on kinematics, power and control, while fabrication of wireless microrobots is fundamentally limited by scaling issues, power and control are often strongly linked [2].

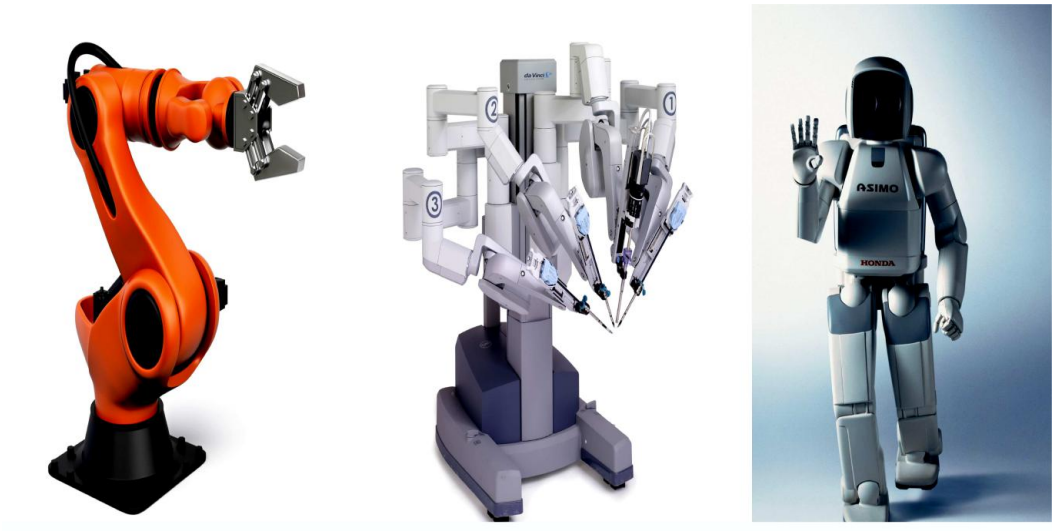

FIGURE 1.1: Macroscale robots including robotic arm (left), da Vinci surgical robot (middle) and Humanoid robots (right).

One of the most critical fields in which microrobots play vital role is the medical field and they are used in therapy and surgeries. Medical microrobots are designed to work in environments such as fluid-filled lumens (i.e., tubes), cavities and soft tissues, the relative changes in the size, geometry and material properties of such environments within a given procedure present design challenges. Consider for example, a microrobot designed to work in the urinary system. The microrobot would be inserted into the urethra and would travel along this lumen to reach the bladder and if the goal is to reach a kidney, the microrobot must first navigate the bladder which is a large open cavity to the microrobot. In order the microrobot can reach the kidney, it must enter the ureter which is a lumen that enters the bladder at an oblique angle and then navigate to the kidney. Thus, designing a microrobot that is capable to negotiate these changing environments is not trivial. Also the fluid flow in the environment of the microrobot presents a significant design challenge. Consider a microrobot designed to work in the circulatory system. In addition to dealing with varying blood-vessel diameter, the microrobot must compete against the pulsating flow of blood which is significant to a small untethered device [2]. The locomotion and localizing of microrobots will be discussed in the next section.

1.1.2 Thesis Overview

Medical microrobots are used to deliver drugs to deep seated places in the human body (circulatory system, central nervous system, urinary system and the fetus) required for the treatment of different diseases.

Several serious diseases affects the deep seated places in the human body such as cancer. Cancer is the second leading cause of death, following heart disease, in many parts of the world [4]. Survival rates are increasing for many types of cancer due to improvements in cancer screening and treatment. This treatment has negative-side effects such as fatigue, pain and blood disorders. These side-effects can be mitigated using targeted drug delivery [2] by localizing the drug only within the vicinity of the diseased region. This localization can be achieved using magnetic drug carriers such as ferromagnetic, superparamagnetic, and paramagnetic particles [5–7]. Motion control of these particles and other microrobotic systems has been only demonstrated using electromagnetic coils with closed-configurations [8]-[14] that cannot be scaled-up to be viable for clinical applications [18].

In this work, point-to-point closed-loop control of the position of the paramagnetic microparticles is achieved using a magnetic-system with an open-configuration. This system allows us to control the position of a permanent magnet and an electromagnetic coil that are fixed to the end-effector of the robotic arm. In addition, the current of the electromagnetic coil is controlled.

The main objective of this work is to control the motion of a microrobot in the form of microparticles to reach a predefined reference, this thesis falls in five chapters. The first of which is a general introduction to this work and also it gives a background on locomotion methods and localization methods used for microrobots. In addition, it presents open and closed configuration

used for the sake of medical applications. Chapter 2 shows the experimental setup used in controlling of the position of microparticles. Chapter 3 discusses the modelling and control of the robotic arm holding the permanent magnet or the electromagnetic coil used in the point to point control of the microparticles. Chapter 4 include the numerical results for controlling the position of the micropaticles in the x-axis and z-axis using permanent magnet and electromagnetic coil. Chapter 5 deals with the conclusion and recommendations for the future work.

1.2 Background

There are several methods used for locomoting and localizing the microrobots. These methods are a little bit stranger than those used with the macroscale robots.

1.2.1 Propulsion Mechanisms of Microrobotic Systems

Microrobots for medical applications needed to be compatible with human body, remotely controllable, smooth in movement, less painful to the patients and capable of performing the designated functions. It is well known that swimming at the microscale requires techniques that differ greatly from those used by macroscale swimmers such as fish and humans. Power must be transduced into motion; to locomote the microrobots within the body. Locomotion

methods of medical microrobots must be designed with their working environment in mind. Thus, they must be designed to work in fluid-filled lumens and cavities and in soft tissues. Microrobot locomotion must also utilize methods that are scale appropriate [2]. A brief description of some propulsion methods are discussed in the following subsections.

1.2.1.1 Helical Propulsion

A number of microswimmer designs use some form of helical propeller shown in Fig. 1.2 for locomotion. Helical propulsion is inspired by bacterial flagella. The method that most closely resembles a bacteria in function uses a rotary motor to turn a passive flagellum. However, miniaturizing such a motor-driven system is difficult. The generation of torque using external magnetic fields has proven to be a successful method for helical propulsion in a number of studies. The magnetic dipole is provided by the head of the helical robot and the rotation under the influence of the rotating magnetic field. Regardless of

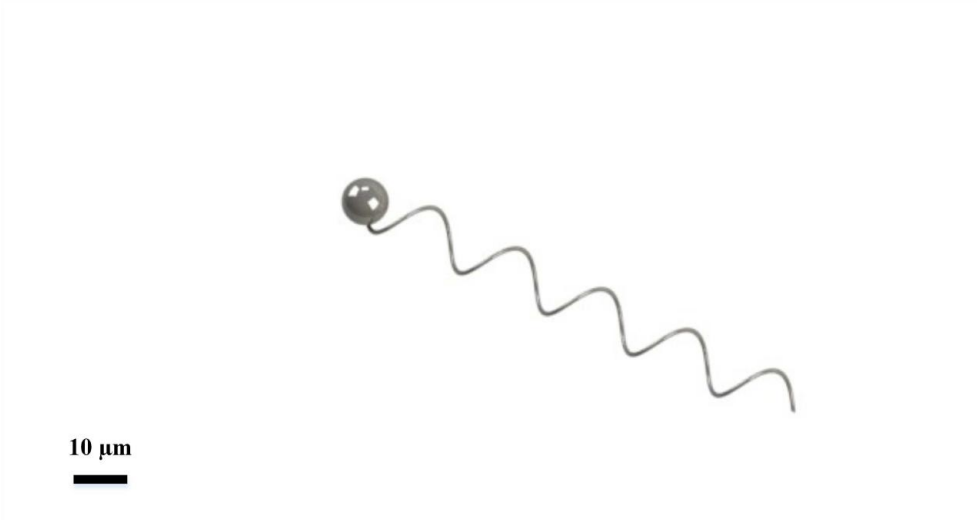

FIGURE 1.2: Helical robot with 10 μm in diameter.

the method used to apply torque, there are options in the fabrication of the helical propeller. The propeller can be made rigid—possibilities range from a simple wire formed into a helix to a multilayer strip that self-forms into a helix because of internal stresses. The efficacy of the propellers is insensitive to the helix cross-section. In rigid propellers, the direction of microrobot motion can be reversed simply by reversing the rotation direction of the magnetic field. That is, rigid propellers are capable of both pushing and pulling a body [2].

1.2.1.2 Traveling-Wave Propulsion

A number of microswimmer designs attempt to create a traveling wave shown in Fig. 1.3 to generate propulsion. Traveling-wave propulsion is inspired by

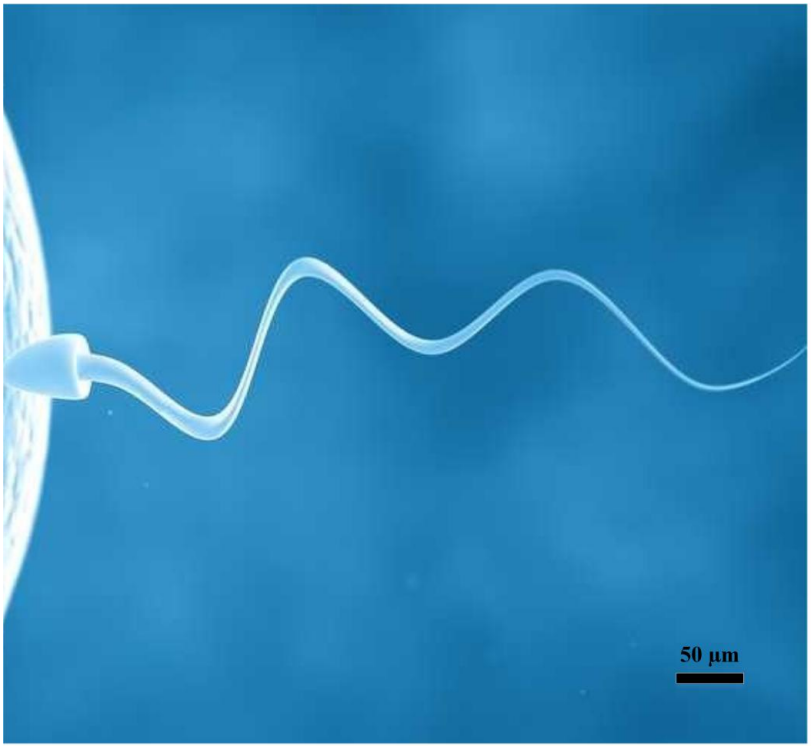

FIGURE 1.3: Traveling wave robot moving under the effect of changing the magnetic field. This picture is from www.businessinsider.com.

eukaryotic flagella. Traveling waves provide an effective means of propulsion at low Reynolds number (R_e) and are even more efficient than helical propellers, assuming equal actuation efficiency. However, implementing a true traveling-wave propeller at the microscale is difficult. Creating the type of distributed actuation seen in eukaryotic flagella is difficult in terms of fabrication, power and control. Some methods create traveling waves without distributed actuation, making microfabrication and wireless control more feasible, but the swimming efficiency is reduced. There several ways to implement the traveling wave propulsion. One of them, to power and control an elastic tail wirelessly with magnetic fields. A field can be used to generate a torque on magnetic material that is rigidly embedded in the microrobot's body. A time-varying oscillating field causes the body to fluctuate, which induces a wave motion in the tail. The mean orientation of the oscillating field dictates the swimming direction of the microrobot. Rather than rigidly connect the magnetic material to the body of the microrobot, one can instead construct an onboard actuator using this type of magnetic method [2].

1.2.1.3 Pulling with Magnetic Field Gradients

Wireless pulling through the use of field gradients is an actuation method that is impossible for autonomous microorganisms and has no direct analogy in nature. Magnetic fields have been used to apply forces and torques on magnetic objects in medical applications. Controlled magnetic fields can be generated in a variety of ways. The first method uses electromagnets that are simultaneously position and current controlled. Grady *et al.* [15] used a single position

controlled electromagnetic coil to control permanent-magnet seed in vivo in a canine brain. Yesin *et al.* [16] superimposed the uniform field of a pair of electromagnetic coils with the gradient field developed by a second pair of coils. The two coil pairs which are rigidly connected, are position controlled to manipulate a magnetic microrobot. The second method uses stationary current-controlled electromagnets. Meeker *et al.* [17] made a helmet configuration which consists of three orthogonal pairs of coils to control magnetic fields throughout a human head, as a stated improvement to the design made by Grady *et al.*. However, this helmet design allows only partial control because full torque and force control is not possible due to the singularities in the workspace. It has also been shown that the electromagnetic coils in a clinical magnetic resonance imaging system (MRI) system can be used to position ferromagnetic beads. The third method uses position-controlled permanent magnets. This is the method used by the Stereotaxis Niobe Magnetic Navigation System, which is used to steer magnetic-tip catheters [2].

Abbott *et al.* [18] had made a comparison between three different propulsion methods (described above) which are: pulling with magnetic field gradients to a submillimeter-sized device [16], rotating magnetic field to helical propeller that mimics a bacterial flagellum in both form and scale [19] and an elastic tail which oscillates behind a magnetic head [20, 21]. He proved that the performance of using helical propeller and elastic tail is better than pulling with magnetic field gradients as microrobot size decreases or as the distance from the magnetic field sources increases for two key reasons. First, although

maximum speed and force generation both decrease as the size of the microrobot is reduced, the decreases are more rapid with field-gradient pulling. Second, it is easier to project magnetic fields over large distances than it is to project field gradients. Also he showed that the best propulsion method in vivo applications is the helical propulsion.

1.2.2 Localization Methods

There are several localization methods used to localize and track a microrobot inside the human body. Every localizing method depends on simple components such as microscopes, cameras, etc combined with image-processing techniques to provide feedback for the closed-loop control system. Spatial resolution is an important factor in the determination of the position of the microrobot. This resolution is indicative of position and/or orientation error, so the resolution is preferably in the submillimeter range for the used microrobots, whose size is a few millimeters at most. Noise- and artifact-robust methods are preferred. The maximum rate at which the position estimation can be updated is also an important factor for real-time control [2].

1.2.2.1 Ultrasound System

The ultrasound system has many advantages: it has no any negative effects on health, low cost as compared to other systems such as magnetic resonance imaging system (MRI) and computed tomography, appropriate resolution and high frame rates which allow for the realization of real-time control.

Khalil *et al.* presented a point to point control for a paramagnetic microparticles in a closed configuration of electromagnetic coils (array of three iron-core electromagnetic coils) using ultrasound as a feedback device. This system accomplished an average position tracking error of 48 μm at an average speed of 191 μm/s [22].

Evertsson *et al.* has developed an algorithm based on quadrature detection and phase gating at the frequency of interest and evaluated the motion of superparamagnetic iron oxide nanoparticles using a high-frequency ultrasound scanner. The developed algorithm provides feedback and controls the motion of nanoparticles using ultrasound feedback [24, 33].

1.2.2.2 Magnetic Resonance Imaging System

The major disadvantage in using magnetic resonance imaging system for tracking and actuation is that it induces time-delay due to communications and interactions between the various modules of the interventional platform. This time-delay may cause instability in the closed-loop control system which will limit the realization of the control system in real-time.

Martel *et al.* controls magnetic drug carriers, nanorobots and magnetotactic bacteria in vivo using magnetic imaging system which provides feedback for the position of these microrobots [11].

1.2.3 Electromagnetic Configurations

Magnetic configurations used with microrobots include: closed and open magnetic configurations.

1.2.3.1 Closed-Configuration of Elecromagnetic Coils

Closed-configurations shown in Fig. 1.4 are those configurations which consist of a number of electromagnetic coils. They are placed in a way to form a closed configuration where the workspace containing the microrobot (e.g., microparticles, helical robot and bacteria) is found between these coils. The

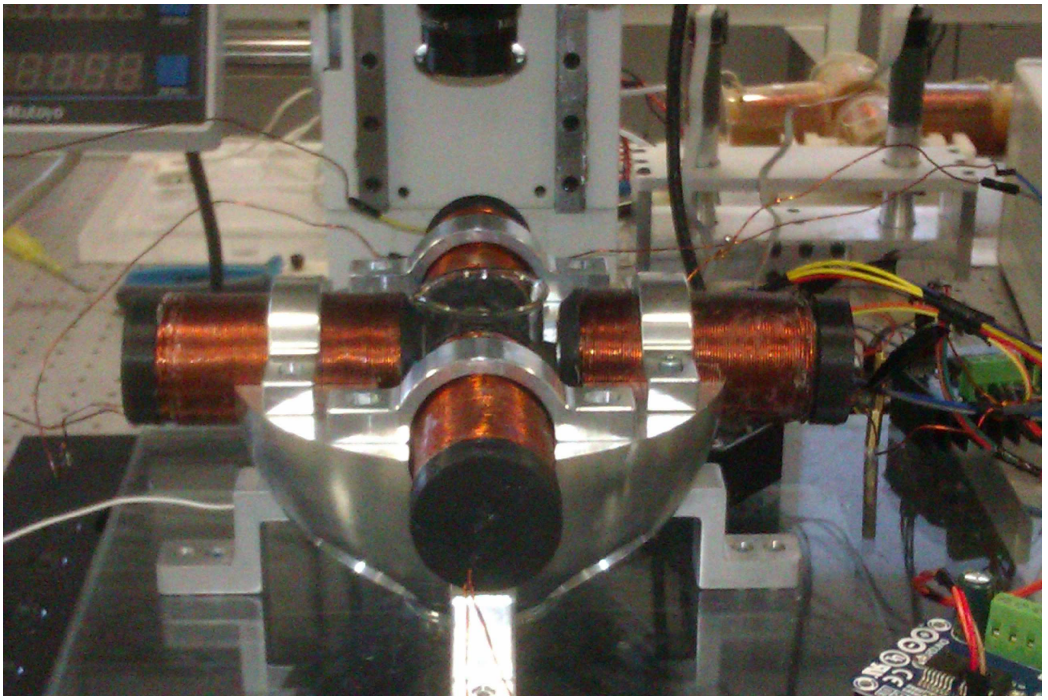

FIGURE 1.4: An electromagnetic system with closed-configuration consists of 4 electromagnetic coils. The microrobot is contained in the center of the electromagnetic configuration. The configuration is placed under a very precise microscope used for feedback.

closed-configurations can not be scaled-up to be used in clinical (real) applications [18] but it is good for the demonstration of many concepts in the microrobotic field.

Microrobots can be in the form of paramagnetic micro/nanoparticles. The advantage of these particles over the other types of microrobots is their small size which give them the opportunity to be used in most clinical applications. However, the magnetic forces of these particles are small due to the dependency of the magnetic force on the size and geometry of the object itself. This problem can be solved by increasing the directional derivatives in the applied field [23].

Khalil *et al.* used a closed configuration of 4 electromagnetic coils to control the motion of microparticles in a fluid (2.4 mm $\times$ 1.8 mm workspace). The microparticles are controlled to move in a certain trajectory (e.g., circular, rectangular and figure-eight paths) using a waypoint control approach (four variables are tuned to reach the desired transient response and decrease settling time) with a maximum steady state position tracking error of 8.6 μm. This motion control is held in the present of static and dynamic obstacles which is achieved using a path planning procedure based on a combination of the potential field and the $A^\star$ approaches [23].

Kummer *et al.* demonstrated a five degree-of-freedom wireless magnetic control of a fully untethered microrobot. He have constructed an electromagnetic system consists of 8 electromagnetic coils (each of 210 mm long and 62 mm

diameter) called OctoMag. Closed-loop control with computer vision is implemented for accurate positioning. The system can be operated with no visual tracking, by a human operator during direct teleoperation depending on visual feedback. The OctoMag was designed for controlling the intraocular microrobots in minimally invasive retinal therapy and diagnosis. It is also used as a wireless micromanipulation system under a light microscope. It is tested to perform wireless vessel puncture of CAM blood vessels in an in vitro chicken embryo [12].

Floyd *et al.* proved that an untethered electromagnetically actuated magnetic microrobot called Mag-μBot (whose dimensions 250 $\times$ 130 $\times$ 100 μm^3) can manipulate microspheres of 50 μm and 230 μm. By using both contact (Mag-μBot is used to push the microspheres physically) and non contact (in which the fluid flow generated by the translation of the Mag-μBot is used to push the microspheres) pushing methods. In his experiments, he used 4 orthogonal electromagnetic coils to prove that [25].

1.2.3.2 Open-Configuration of Elecromagnetic Coils

Open-configurations are the configurations which contain permanent magnet or electromagnetic coil, arranged in way such that the system can be applied in real clinical applications.

Fountain *et al.* [26] has proposed using non uniform magnetic fields with helical

microrobots instead of using uniform magnetic fields produced from orthogonal arrangement of electromagnetic coils. The non uniform magnetic fields are generated using rotating permanent magnet. The complexity of the human body gives a great importance to these fields as this open configuration helps helical microrobots to be used in hard-to-reach places in the body. Unlike the closed configuration which cannot be scaled-up to be used in such critical application.

Mahoney *et al.* [27, 28] have proposed a combination of magnetic field-driven helical robots [29, 30] and a robotic arm. The helical robot (with length and diameter of 26 mm and 18 mm, respectively) overcomes the problem of the limited projection distance of the magnetic field gradient, whereas the robotic arm (with open-configuration) holds a permanent magnet and generates rotating dipole field over a large workspace, as opposed to electromagnetic coils with closed-configurations. Therefore, this combination allows magnetic-based manipulation systems to be scaled-up and used in diverse biomedical applications [31]. It has also been demonstrated that the attractive forces acting on a magnetic microrobot can be converted into a lateral force by rotating the actuator dipole according to an open-loop trajectory [32].

In this thesis, point-to-point closed-loop control of paramagnetic microparticles is achieved in three-dimensional (3D) space using a magnetic-system with an open-configuration. A conceptual image of wireless control of paramagnetic microparticles carrying the drug using a robotic arm and the magnetic field generated from a permanent magnet or an electromagnetic coil to deliver the

drug to the diseased cell in the vertebral column, is shown in Fig. 1.5.Constant magnetic field is used in this work, unlike the varying magnetic field resulting from the rotating magnetic field done by Mahoney *et al.*. This system allows controlling the position and orientation of a permanent magnet or an electromagnetic coil that are fixed to the end-effector of the robotic arm. The motion control is achieved such that the microparticles is localized at the reference position without contact with the surrounding glass tube. This motion control is achieved by pulling the paramagnetic microparticles towards a reference position (x- and z-positions) using the magnetic field gradients. These gradient are controlled using two methods. The first method depends on controlling the position of the permanent magnet with respect to the position of the microparticle and the given reference position. The second method depends on

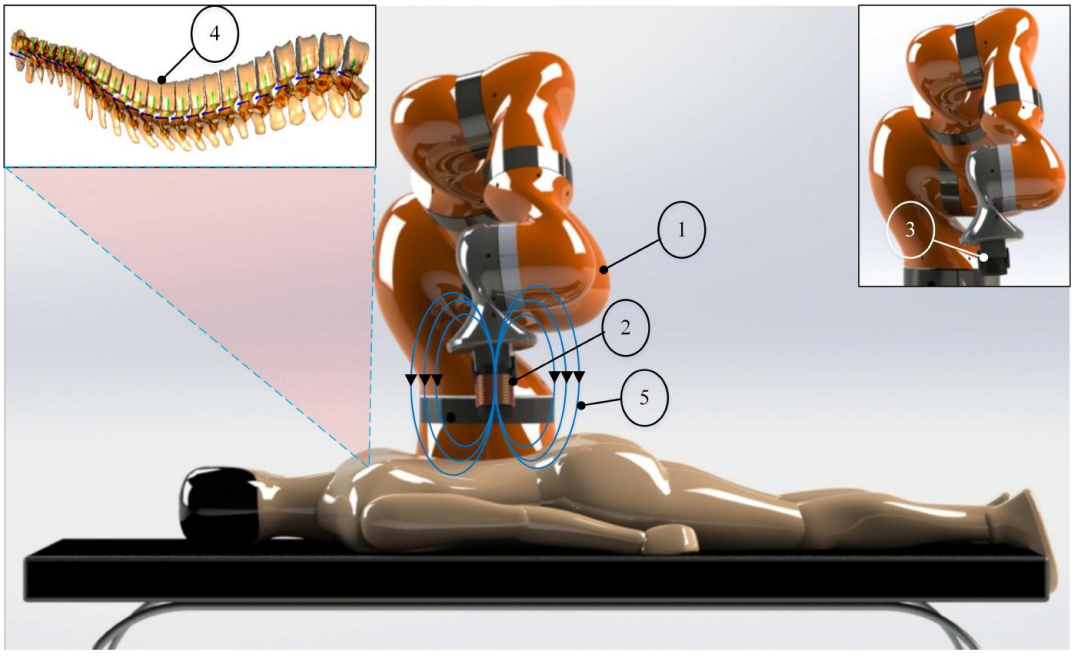

FIGURE 1.5: A schematic representation of the wireless control of paramagnetic microparticles carrying the drug using a robotic arm ① and the magnetic field ⑤ generated from an electromagnetic coil ② or a permanent magnet ③ to deliver the drug to the diseased cell in the vertebral column ④.

controlling the position and the input current of an electromagnetic coil.

Chapter 2

Magnetic-Based Robotic System

The magnetic-based robotic system presented in our work is shown in Fig. 2.1, that is used for controlling the motion of paramagnetic microparticles ① wirelessly. The inset in the figure shows a pair of microparticles moving towards a reference position (red crosshair) under the influence of the controlled magnetic field gradient. A permanent magnet ② is fixed to the end-effector ③ of the robotic arm. The microparticles ① are contained in water inside a glass tube ④ and are tracked using a microscopic system ⑤. The permanent magnet generates maximum magnetic fields of 85 mT. The white square indicates the microparticles and is assigned using a feature tracking algorithm. An electromagnetic coil ⑥ (inset in the upper-left corner) can be also attached to the end-effector of the robotic arm ⑦. The electromagnetic coil generates magnetic field of 7.5 mT for current input of 0.6 A. The workspace of the magnetic-based robotic system is 200 mm, 20 mm, and 20 mm along x-, y-,

and z-axis, respectively. The control of the system is implemented using Matlab Simulink.

The robotic arm used in the magnetic-based robotic system is shown in Fig. 2.2.

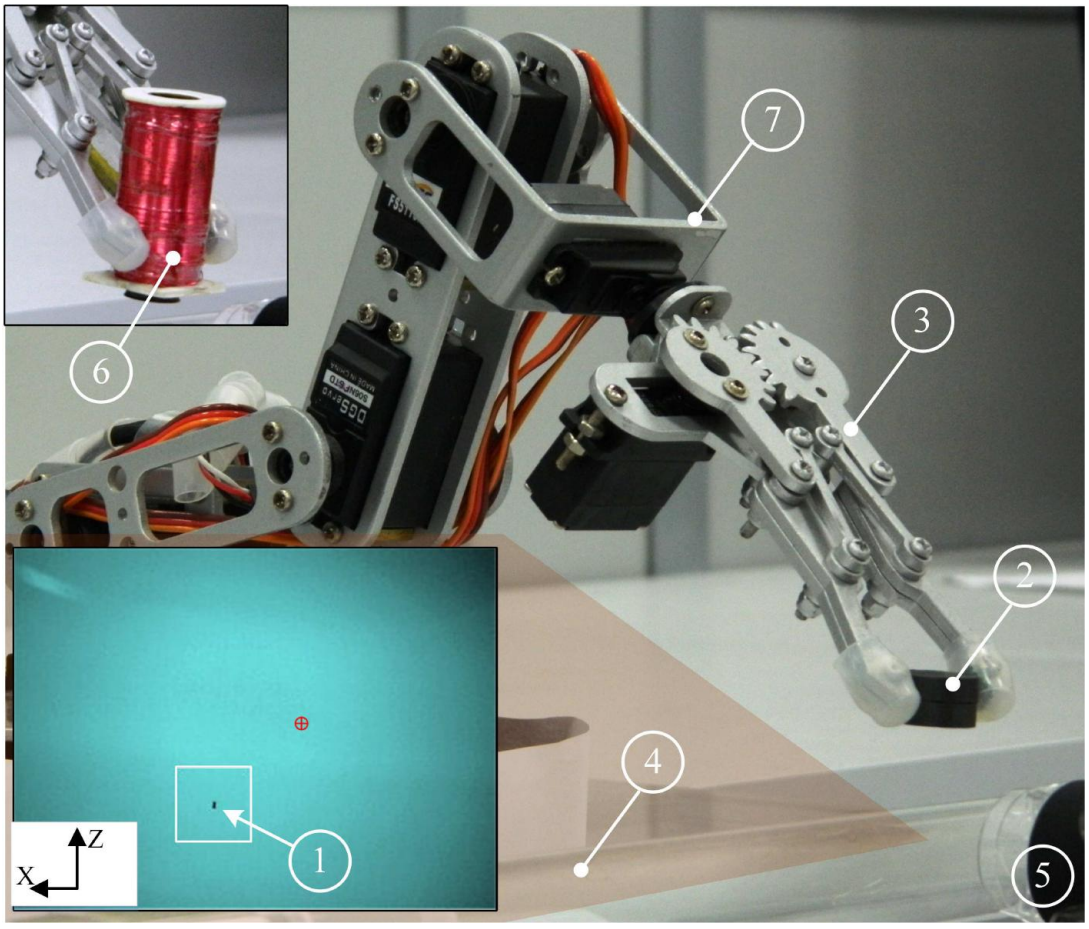

FIGURE 2.1: A magnetic-based robotic system for the wireless motion control of paramagnetic microparticles ①. The inset shows a pair of microparticles moving towards a reference position (red crosshair) under the influence of the controlled magnetic field gradient. A permanent magnet ② is fixed to the end-effector ③ of the robotic arm. The microparticles are contained in water inside a glass tube ④ and are tracked using a microscopic system ⑤. The permanent magnet generates maximum magnetic fields of 85 mT. The white square indicates the microparticles and is assigned using a feature tracking algorithm. An electromagnetic coil ⑥ (inset in the upper-left corner) can be also attached to the end-effector of the robotic arm ⑦. The electromagnetic coil generates magnetic field of 7.5 mT for current input of 0.6 A.

It has 6 servo motors (Appendix B), but it is modeled as 4 DOF robotic arm as the last two servo motors are not used in our experiments. Thus these two servo motors are set to a certain angle and not changed throughout the experiments, one of them is controlling the orientation of the end-effector (the end-effector is always parallel to the glass tube) and the other one is responsible for opening and closing the gripper of the robotic arm. The 4 DOF robotic arm contains 4 revolute joints. A servo motor (input voltage: $4.8 \sim 6$ V) is connected to every revolute joint, each motor has 3 wires. The 1^{st} wire is connected to +5 V of the power supply, 2^{nd} wire is the control signal that determines the value of the angle by which the motor will rotate and the 3^{rd} wire is connected to the ground. The control signal of the servo motor (2^{nd} wire) is connected to an Arduino control board (Arduino Mega 2560, Arduino, Memphis, Tennessee, U.S.A). The end-effector of this robotic arm can be adapted to hold a permanent magnet or an electromagnetic coil.

The glass tube emulates the vertebral column in the human body that may contains the tumor. It is filled with water that resembles the cerebrospinal fluid found inside the vertebral column as both of them approximately has the same viscosity. The diameter of the glass tube is 40 mm which is the average diameter of the vertebras of the vertebral column. It contains the microparticles that is controlled either by a permanent magnet or by an electromagnetic coil.

The microparticles (Appendix A) are paramagnetic with saturation magnetization of 6.6×10^{-3} Am^2/g, consisting of iron-oxide in a poly (lactic acid) matrix (PLAParticles-M-redF-plain from Micromod Partikeltechnologie GmbH, Rostock-Warnemuende, Germany). The diameter of a microparticle (d_p) is 100 μm and its density (ρ) is 1.4×10^3 kg/m^3. In real medical application, these microparticles are those who will carry the drug to the places that will have the tumor.

Position of the microparticles is determined using a digital microscope (Appendix C) which gives a live stream video and a feature tracking algorithm that tracks the micropaticle. Its magnification range is from (20x-200x) so it is suitable view the microparticle whose diameter is 100 μm. The field-of-view of the microscopic system is set to 10 mm, 10 mm, and 10 mm along x-, y-,

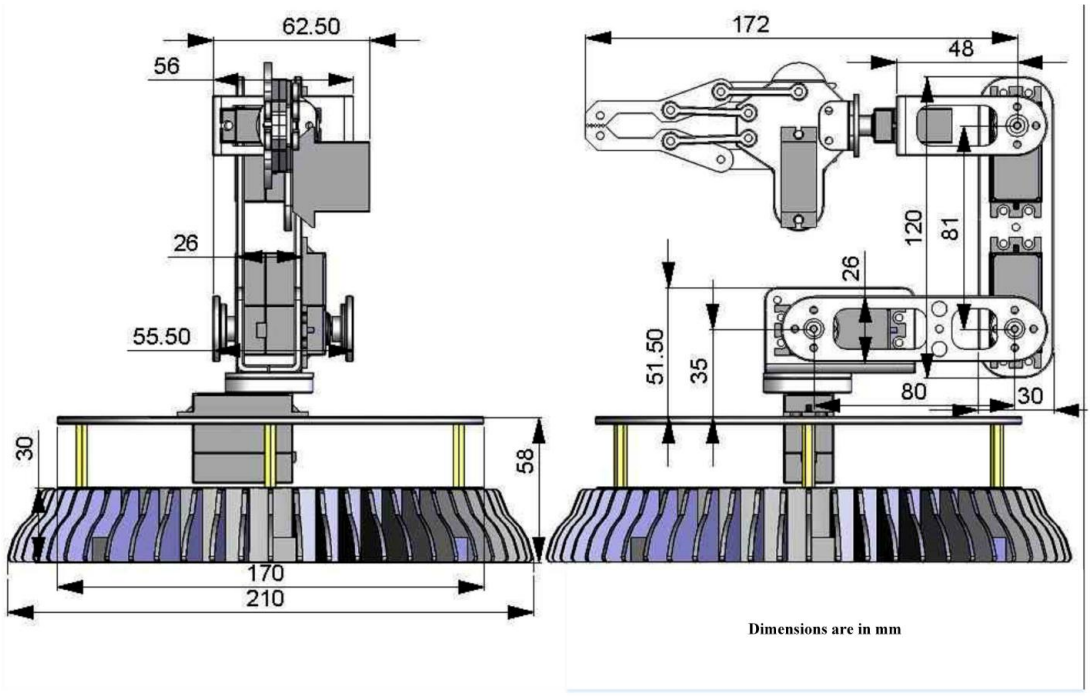

FIGURE 2.2: 4 DOF robotic arm dimensions.

TABLE 2.1: Specifications of the magnetic-based robotic system using permanent magnet. The magnetic fields are measured at the center of the workspace using a calibrated 3-axis digital Teslameter (Senis AG, 3MH3A-0.1%-200mT, Neuhofstrasse, Switzerland).

Parameter	**Value**	**Parameter**	**Value**
$\|\mathbf{B}(\mathbf{P})\|$ [mT]	85	$\nabla\|\mathbf{B}(\mathbf{P})\|$ [T.m^{-1}]	1.62
$B_x(\mathbf{P})$ [mT]	39.4	$\frac{\partial B(\mathbf{P})}{\partial x}$ [T.m^{-1}]	0.49
$B_y(\mathbf{P})$ [mT]	38.2	$\frac{\partial B(\mathbf{P})}{\partial y}$ [T.m^{-1}]	0.37
$B_z(\mathbf{P})$ [mT]	64.5	$\frac{\partial B(\mathbf{P})}{\partial z}$ [T.m^{-1}]	1.52

and z-axis, respectively.

The magnetic field generated from the magnetic-based robotic system, is generated from a permanent magnet or from an electromagnetic coil. The characterization of the magnetic field generated from them is discussed in the following two sections.

2.1 Permanent Magnet

A permanent magnet is fixed to the end-effector of the robotic arm, used to control the position of the microparticles in the x- and z-axes. The permanent magnet is made of ceramic material, its dimension is 18 mm×5 mm. The maximum magnetic fields generated using the parament magnet is 85 mT. The maximum magnetic field gradients of the permanent magnet within the workspace of the system are calculated to be 1.6 T/m. Fig. 2.3 shows the magnetic fields generated using the permanent magnet within a workspace of 10 mm×10 mm. These magnetic fields are measured at the center of the

workspace using a calibrated 3-axis digital Teslameter (Senis AG, 3MH3A-0.1%-200mT, Neuhofstrasse, Switzerland) at fine grid that span the workspace of the microparticles. The permanent magnet is fixed with a parallel configuration to z-axis using the end-effector of the robotic arm. The magnetic fields are measured by moving the probe of the Teslameter using a planar motion stage throughout the workplace of the microparticle (indicated using the red arrow). The permanent magnet generates magnetic fields of 5 mT, 5 mT, and 12 mT along x-, y-, and z-axis, respectively, at 10 mm along x_p. x_i, y_i, z_i represent the frames of the robotic arm, for $i = 1, 2, 3$. Further, x_j, y_j, z_j

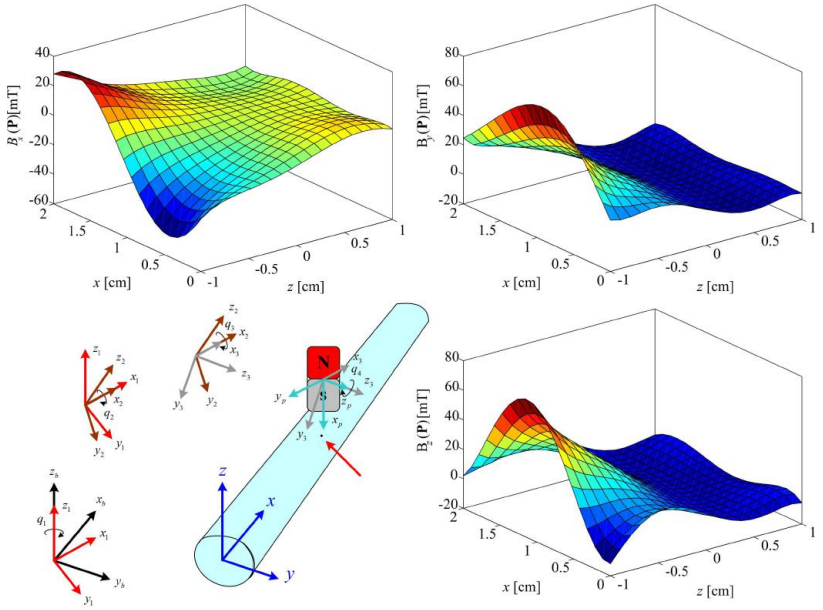

FIGURE 2.3: The magnetic fields generated using a permanent magnet along x-, y-, and z-axis. The permanent magnet is fixed with a parallel configuration to z-axis using the end-effector of the robotic arm. The magnetic fields are measured by moving the probe of the Teslameter using a planar motion stage throughout the workplace of the microparticle (indicated using the red arrow). The permanent magnet generates magnetic fields of 5 mT, 5 mT, and 12 mT along x-, y-, and z-axis, respectively, at 10 mm along x_p. x_i, y_i, z_i represent the frames of the robotic arm, for $i = 1, 2, 3$. Further, x_j, y_j, z_j represent the base and permanent magnet frames for $j = b$ and p, respectively. q_k are the generalized-coordinates of the robotic arm, for $k = 1, \ldots, 4$..

represent the base and permanent magnet frames for $j = b$ and p, respectively. q_k are the generalized-coordinates of the robotic arm, for $k = 1, \ldots, 4$. Fifth order polynomials (yield minimum sum squares for error) are used to provide best fits for the measured magnetic fields along x-, y- and z-axis. The permanent magnet provides maximum magnetic fields of 45 mT, 70 mT, and 75 mT along x-, y- and z-axis, respectively. Within the vicinity of the workspace (10 mm×10 mm) of the microparticles, the magnetic field components are 5 mT, 5 mT, and 12 mT along x-, y- and z-axis, respectively. Characteristics of the magnetic-based robotic system are provided in Table 2.1.

2.2 Electromagnetic Coil

The robotic arm is adapted to hold the electromagnetic coil in its end-effector, used to control the position of the microparticles in the x- and z-axes. The number of turns of the coil is about 1600 turn. The coil has two wires connected to the +ve and -ve output terminal of the driver board (Appendix D), which is connected to the control signal of the Arduino control board and also connected to a power supply of 12 V. The electromagnetic coil is fixed with a parallel configuration to z-axis using the end-effector of the robotic arm. The magnetic fields are measured by moving the probe of the Teslameter using a planar motion stage throughout the workplace of the microparticle (indicated using the red arrow). x_i, y_i, z_i represent the frames of the robotic arm, for $i = 1, 2, 3$. Further, x_j, y_j, z_j represent the base and electromagnetic coil frames for $j = b$ and c, respectively. q_k are the generalized-coordinates of the

robotic arm, for $k = 1, \ldots, 4$. The maximum magnetic fields generated using the electromagnetic coil is 7.5 mT. The maximum magnetic field gradients generated from the electromagnetic coil within the workspace of the system are calculated to be 0.9 T/m as shown in Table 2.2. The magnetic fields generated using the electromagnetic coil with the configuration shown in Fig. 2.4. The magnetic field components are 4 mT, 4 mT, and 5 mT along x-, y-, and z-axis, respectively, at 10 mm along x_p and for an input current of 0.6 A.

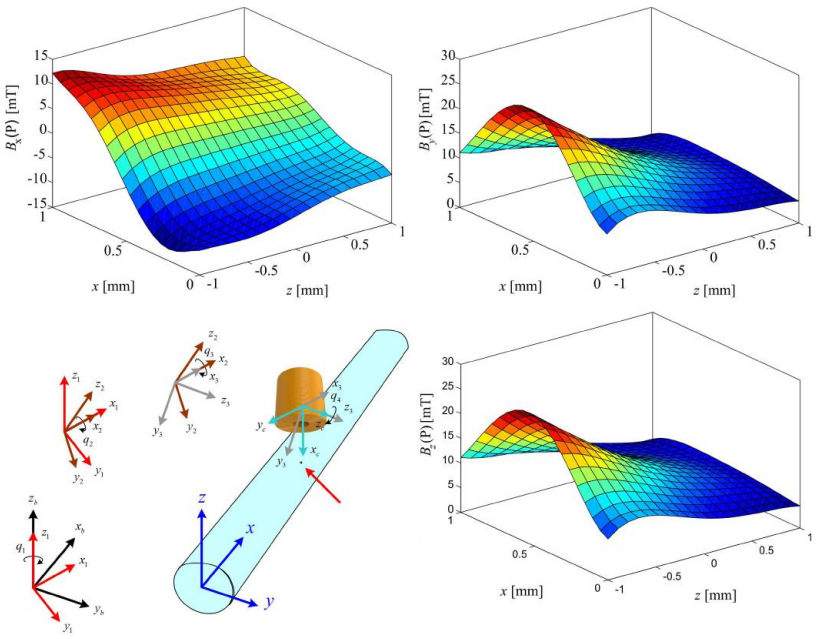

FIGURE 2.4: The magnetic fields generated using a permanent magnet along x-, y-, and z-axis. The permanent magnet is fixed with a parallel configuration to z-axis using the end-effector of the robotic arm. The magnetic fields are measured by moving the probe of the Teslameter using a planar motion stage throughout the workplace of the microparticle (indicated using the red arrow). The electromagnetic coil generates magnetic fields of 4 mT, 4 mT, and 5 mT along x-, y-, and z-axis, respectively, at 10 mm along x_p. The input current to the coil is 0.6 A. x_i, y_i, z_i represent the frames of the robotic arm, for $i = 1, 2, 3$. Further, x_j, y_j, z_j represent the base and permanent magnet frames for $j = b$ and c, respectively. q_k are the generalized-coordinates of the robotic arm, for $k = 1, \ldots, 4$.

TABLE 2.2: Specifications of the magnetic-based robotic system using an electromagnetic coil. The magnetic fields are measured at the center of the workspace using a calibrated 3-axis digital Teslameter (Senis AG, 3MH3A-0.1%-200mT, Neuhofstrasse, Switzerland).

Parameter	**Value**	**Parameter**	**Value**
$\max I_i$ [A]	0.6	Number of turns	1600
$\lvert\mathbf{B}(\mathbf{P})\rvert$ [mT]	7.5	$\nabla\lvert\mathbf{B}(\mathbf{P})\rvert$ [T.m^{-1}]	0.9
$B_x(\mathbf{P})$ [mT]	4.0	$\frac{\partial B(\mathbf{P})}{\partial x}$ [T.m^{-1}]	0.38
$B_y(\mathbf{P})$ [mT]	4.0	$\frac{\partial B(\mathbf{P})}{\partial y}$ [T.m^{-1}]	0.29
$B_z(\mathbf{P})$ [mT]	5.0	$\frac{\partial B(\mathbf{P})}{\partial z}$ [T.m^{-1}]	0.76

Chapter 3

Modeling and Control of the Magnetic-Based Robotic System

In the magnetic-based robotic system, the position of the microparticles which are moving in the fluid inside the glass tube is controlled using the magnetic field. This magnetic field is either generated from a permanent magnet or from an electromagnetic coil. In case of controlling the position using a permanent magnet, the robotic arm is the actuator. However, in case of controlling the position using an electromagnetic coil, both the robotic arm and the coil are the actuators. In order to control this system, the robotic arm and the forces acting on the microparticle are modelled.

3.1 Modeling of the Magnetic-Based Robotic System

The dynamical model of the magnetic-based robotic system includes: modeling of the robotic arm (forward and inverse kinematics) and modeling of the forces exerted on the microparticle.

3.1.1 Modeling of the Robotic Arm

The problem of kinematics is to describe the motion of the manipulator without consideration of the forces and torques, therefore the kinematic description is a geometric one. The modeling of robotic arm comes in two steps. The first step is formulating the forward kinematics, which means determining the position and orientation of the end-effector given the values for the joint variables of the robot. Second step is formulating the inverse kinematics, that concerns determining the values of the joint variables given the end-effector position and orientation [34].

A robot manipulator is composed of a set of links connected together by joints. The joints can be very simple such as a revolute joint or a prismatic joint or they can be more complex such as a ball and socket joint (a revolute joint is like a hinge and allows a relative rotation about a single axis and a prismatic joint permits a linear motion along a single axis which can be an extension or retraction). The difference between the simple and complex joints is that the

simple joints have only a single degree-of-freedom (DOF) of motion: the angle of rotation in the case of a revolute joint and the amount of linear displacement in the case of a prismatic joint. However, the complex joints have two DOF [34].

A robot manipulator with n joints will have $n + 1$ links, since each joint connects two links. Since the robotic arm used in this work is 4 DOF, so it has 4 revolute joints and 5 links. The joints are numbered from 1 to n, while the links are numbered from 0 to n starting from the base. By this convention, joint i connects link $i - 1$ to link i. The location of joint i is considered to be fixed with respect to link $i - 1$. When joint i is actuated, link i moves. Therefore, link 0 (the first link) is fixed and does not move when the joints are actuated. A joint variable denoted by q_i is associated with the i^{th} joint. In the case of a revolute joint, q_i is the angle of rotation (θ_i) and in the case of a prismatic joint, q_i is the joint displacement d_i. To perform the kinematic analysis, a coordinate frame is rigidly attached to each link. In particular, we attach $o_i x_i y_i z_i$ to link i. This means that, whatever motion the robot executes the coordinates of each point on link i are constant when expressed in the i^{th} coordinate frame. Furthermore, when joint i is actuated, link i and its attached frame $o_i x_i y_i z_i$ experience a resulting motion. The frame $o_0 x_0 y_0 z_0$ which is attached to the robot base, is referred to as the inertial frame [34].

3.1.1.1 Forward Kinematics of the Robotic Arm

The forward or configuration kinematic equations for rigid robots is concerned with the relationship between the individual joints of the robot manipulator and the position and orientation of the end-effector. The joint variables are the angles between the links in the case of revolute or rotational joints and the link extension in the case of prismatic or sliding joints. Forward kinematics is used to determine the position and orientation of the end-effector given the values for the joint variables of the robot [34].

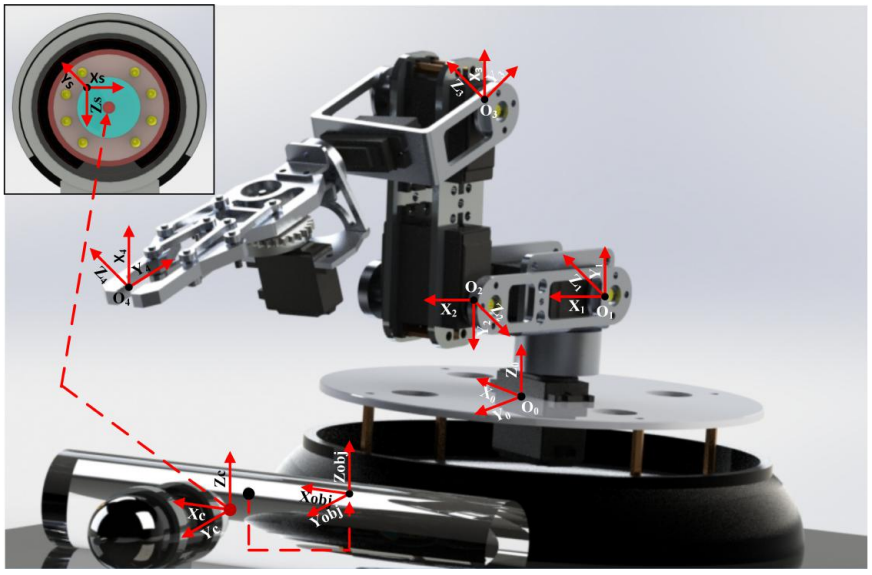

FIGURE 3.1: Magnetic-based robotic system for the wireless motion control of paramagnetic microparticles including all the frame of references. X_0, Y_0, Z_0 is the world reference frame fixed to the first revolute joint (the base of the robotic arm), $X_1Y_1Z_1$ is the frame fixed to the second revolute joint, X_2, Y_2, Z_2 is the frame fixed to the third revolute joint, X_3, Y_3, Z_3 is the frame fixed to the fourth revolute joint, X_4, Y_4, Z_4 is the frame fixed to the end-effector of the robotic arm, X_{obj}, Y_{obj}, Z_{obj} is the frame fixed to the microparticle, X_c, Y_c, Z_c is the frame fixed to the center of the digital microscope and X_s, Y_s, Z_s is the frame fixed to the upper-left corner of the digital microscope (inset in the upper-left corner).

The convention used in this work for selecting frames of reference of the robotic arm is the Denavit-Hartenberg (DH) convention [34]. The DH representation has became the standard way of representing robots and modelling their motions. It is then possible to realate one joint to the next and ultimately to assemble a complete representation of a robot's geometry. The fundamental problem of DH representation is that all the motions are about the x- and z-axes, the method can not represent any motion about the y-axis. Therefore if there is any motion about y-axis, the DH method will fail. This occurs in a number of circumstances for example, suppose two joint axes that are supposed to be parallel are assembled with a slight deviation. The small angle between the two axes will require a motion about the y-axis. Since the robotic arm used in this work, does not contain any two parallel joints thus the DH convention will work perfectly.

After putting every joint in its zero position. The DH method begins with a systematic approach in assigning and labelling an orthonormal (X, Y and Z) coordinate system to each robot joint as shown in Fig. 3.1 in the following way:

Step 1: a number is given for every joint from 1 to N starting with the base and ending with the end-effector yaw, pitch and roll in that order. Step 2: z-axis is established for each joint. if the joint is revolute, the z-axis is in the direction of rotation as followed by the right-hand rule for rotations. While if the joint is prismatic, the z-axis for the joint is along the direction of the linear movement. In each case the index number for the z-axis of joint n (as well as the local reference frame for the joint) is $n-1$. Step 3: the origin of the

coordinate system of the base O_0 is established and X_0, Y_0 is chosen to form cartesian coordinate system. Since the first frame (frame 0) is at the base of the robotic arm, and therefore, there are no joints before it, the direction of X_0 is arbitrary. For convenience (only), it is chosen to be assigned in the same direction as the x-axis in the world frame. There is no problem if another direction is chosen. Step 4: from 1 to N, the origin O_i is established in the intersection of Z_i with the common normal to Z_{i-1} and Z_i. If they do not intersect, the intersection of Z_i with a common normal between Z_i and Z_{i-1} is used (If parallel, O_i is placed in joint $i+1$). Step 5: X_i is established as common normal to Z_{i-1} and Z_i. In other words, X_i is selected to be orthogonal to both Z_i and Z_{i-1}. If Z_i and Z_{i-1} are parallel, point X_i is placed away from Z_{i-1} [34].

Then the DH parameters are derived for every joint as shown in Table 3.1 [34]. Where θ_i is the joint angle and it is found by rotating over z_{i-1} to make x_{i-1} parallel to x_i, d_i is the link offset and it is acquired by translating over z_{i-1} to make x_{i-1} and x_i aligned, a_i is the link length and it is gotten by translating over x_i to make o_{i-1} and o_i coincide and α_i is the link twist and it obtained by rotating over x_i to align z_{i-1} with z_i. L_1 is the length of the first link (distance from O_0 to O_1), L_2 is the length of the second link (distance from O_1 to O_2), L_3 is the length of the third link (distance from O_2 to O_3) and L_4 is the length of the forth link (distance from O_3 to O_4).

Finally The transformation matrix $^{\mathbf{i-1}}\mathbf{A_i}$ is used to relate any frame i to the

TABLE 3.1: The DH parameters for every joint in the 4 DOF robotic arm. θ_i is the joint angle, d_i is the link offset, a_i is the link length, α_i is the link twist, L_1 is the length of the first link, L_2 is the length of the second link, L_3 is the length of the third link and L_4 is the length of the forth link.

i	θ_i	d_i	a_i	α_i
1	θ_1	L_1	0	90°
2	θ_2	0	L_2	180°
3	$\theta_3 - 90°$	0	L_3	180°
4	$\theta_4 - 150°$	0	L_4	0°

frame previous to it $i-1$ and it is found in the following form [34]:

$$ {}^{\mathbf{i-1}}\mathbf{A_i} = \begin{bmatrix} C\theta_i & -C\alpha_i S\theta_i & S\alpha_i S\theta_i & a_i C\theta_i \\ S\theta_i & C\alpha_i C\theta_i & -S\alpha_i C\theta_i & a_i S\theta_i \\ 0 & S\alpha_i & C\alpha_i & d_i \\ 0 & 0 & 0 & 1 \end{bmatrix}, \tag{3.1} $$

where $C\theta_i$ stands for $\cos\theta_i$ and $S\theta_i$ stands for $\sin\theta_i$. As the robotic arm used here is 4 DOF robot, thus 4 transformation matrices are required to relate the inertial frame (base frame) to end-effector frame. ${}^{\mathbf{0}}\mathbf{A_1}$ is the transformation matrix which relates inertial frame to the 1st frame and it is calculated by substituting with the values found in Table 2.1 in equation (3.1):

$$ {}^{\mathbf{0}}\mathbf{A_1} = \begin{bmatrix} C\theta_1 & 0 & S\theta_1 & 0 \\ S\theta_1 & 0 & -C\theta_1 & 0 \\ 0 & 1 & 0 & 2.5 \\ 0 & 0 & 0 & 1 \end{bmatrix}, \tag{3.2} $$

$^{\mathbf{1}}\mathbf{A_2}$ is the transformation matrix which relates 1st frame to the 2st frame:

$$^{\mathbf{1}}\mathbf{A_2} = \begin{bmatrix} C\theta_2 & S\theta_2 & 0 & 8C\theta_2 \\ S\theta_2 & -C\theta_2 & 0 & 8S\theta_2 \\ 0 & 0 & -1 & 0 \\ 0 & 0 & 0 & 1 \end{bmatrix}, \tag{3.3}$$

$^{\mathbf{2}}\mathbf{A_3}$ is the transformation matrix which relates 2st frame to the 3st frame:

$$^{\mathbf{2}}\mathbf{A_3} = \begin{bmatrix} S\theta_3 & -C\theta_3 & 0 & 8S\theta_3 \\ -C\theta_3 & -S\theta_3 & 0 & -8C\theta_3 \\ 0 & 0 & -1 & 0 \\ 0 & 0 & 0 & 1 \end{bmatrix}, \tag{3.4}$$

$^{\mathbf{3}}\mathbf{A_4}$ is the transformation matrix which relates 3st frame to the 4st frame:

$$^{\mathbf{3}}\mathbf{A_4} = \begin{bmatrix} -\frac{\sqrt{3}}{2}C\theta_4 + \frac{1}{2}S\theta_4 & \frac{\sqrt{3}}{2}S\theta_4 + \frac{1}{2}C\theta_4 & 0 & -\frac{17\sqrt{3}}{2}C\theta_4 + \frac{17}{2}S\theta_4 \\ -\frac{\sqrt{3}}{2}S\theta_4 - \frac{1}{2}C\theta_4 & -\frac{\sqrt{3}}{2}C\theta_4 + \frac{1}{2}S\theta_4 & 0 & -\frac{17\sqrt{3}}{2}S\theta_4 - \frac{17}{2}C\theta_4 \\ 0 & 0 & 1 & 0 \\ 0 & 0 & 0 & 1 \end{bmatrix}, \tag{3.5}$$

Thus the transformation between the base frame (B) and the end-effector frame (E) $^{\mathbf{B}}\mathbf{T_E}$ can be calculated as shown:

$$^{\mathbf{B}}\mathbf{T_E} = ^{\mathbf{0}}\mathbf{A_4} = ^{\mathbf{0}}\mathbf{A_1}\ ^{\mathbf{1}}\mathbf{A_2}\ ^{\mathbf{2}}\mathbf{A_3}\ ^{\mathbf{3}}\mathbf{A_4}, \tag{3.6}$$

While the original matrix of ${}^{\mathbf{B}}\mathbf{T}_{\mathbf{E}}$ is:

$$ {}^{\mathbf{B}}\mathbf{T}_{\mathbf{E}} = \begin{bmatrix} n_x & o_x & a_x & P_x \\ n_y & o_y & a_y & P_y \\ n_z & o_z & a_z & P_z \\ 0 & 0 & 0 & 1 \end{bmatrix}, \tag{3.7} $$

Where P_x, P_y and P_z are the position of the end-effector in the x-, y- and z-axes respectively. While n_x, o_x and a_x is the orientation of the end-effector around x-axis, and n_y, o_y and a_y is the orientation of the end-effector around y-axis and n_z, o_z and a_z is the orientation of the end-effector around z-axis. Therefore if the 4 thetas (θ_1, θ_2, θ_3 and θ_4) are given, by equating equations (3.7) and (3.6) the position and orientation of the end-effector is found.

3.1.1.2 Inverse Kinematics of the Robotic Arm

Inverse kinematics concerns with determining the values of the joint variables given the end-effector position and orientation. Thus in order to reach to a specific point with x-, y- and z-coordinates in the space, inverse kinematics of the robotic arm is implemented using feedback stabilization method.

The kinematic equation of the end-effector of the robotic arm is shown in the position and velocity levels respectively:

$$ \mathbf{x} = \phi(\mathbf{q}) \quad \text{and} \quad \dot{\mathbf{x}} = \mathbf{J}(\mathbf{q})\dot{\mathbf{q}}, \tag{3.8} $$

where $\mathbf{x} = \begin{bmatrix} x & y & z \end{bmatrix}^{\mathrm{T}}$ is the generalized coordinates of the task-space, and x, y and z represent the frames of the end-effector. Further, $\mathbf{q} = \begin{bmatrix} \theta_1 & \theta_2 & \theta_3 & \theta_4 \end{bmatrix}^{\mathrm{T}}$ is a vector of generalized coordinates, and θ_k are the thetas of the revolute joints of the robotic arm, for $k = 1, \ldots, 4$. Further, $\phi(\mathbf{q})$ is the forward kinematics equation of the position of the end-effector and $\mathbf{J}(\mathbf{q})$ is the Jacobian matrix of the robotic arm and the Jacobian matrix for a 4 DOF robotic arm is given by the following matrix:

$$\mathbf{J}(\mathbf{q}) = \begin{bmatrix} \frac{\partial x}{\partial \theta_1} & \frac{\partial x}{\partial \theta_2} & \frac{\partial x}{\partial \theta_3} & \frac{\partial x}{\partial \theta_4} \\ \frac{\partial y}{\partial \theta_1} & \frac{\partial y}{\partial \theta_2} & \frac{\partial y}{\partial \theta_3} & \frac{\partial y}{\partial \theta_4} \\ \frac{\partial z}{\partial \theta_1} & \frac{\partial z}{\partial \theta_2} & \frac{\partial z}{\partial \theta_3} & \frac{\partial z}{\partial \theta_4} \end{bmatrix}. \tag{3.9}$$

The position of the end-effector is used to calculate the generalized coordinates (thetas) at the joint space by integrating the kinematical equation in the velocity level (3.8). However, integration of (3.8) can result in increasing any initial error with time. Therefore, feedback stabilization approach is used to guarantee that integration of (3.8) will not magnify the initial error. This integration is done by setting, $\dot{\mathbf{q}} \longmapsto \mathbf{J}^{-1}(\mathbf{q})\mathbf{K}\mathbf{s}$, to achieve stable integration of (3.8).

$$\dot{\mathbf{q}} = \mathbf{J}^{-1}(\mathbf{q})\mathbf{K}\mathbf{s}. \tag{3.10}$$

where $\mathbf{J^{-1}(q)}$ is the inverse of the Jacobian matrix. It is not calculated using the normal inverse method but it is calculated using pseudoinverse formula shown in equation (3.11) as the Jacobian matrix of 4 DOF robotic arm is a matrix of 3 rows and 4 columns which is not a square matrix. Thus the inverse

of the Jacobian matrix can not be calculated using the inverse methods.

$$\mathbf{J^{-1}(q) = J^{T}(q)(J(q)J^{T}(q))^{-1}}, \tag{3.11}$$

while $\mathbf{K}$ is a positive-definite matrix, and $\mathbf{s}$ is given by:

$$\mathbf{s} = \mathbf{x_r} - \phi(\mathbf{q}), \tag{3.12}$$

where $\mathbf{s}$ is the error calculated between the $\mathbf{x_r} = \begin{bmatrix} x_r & y_r & z_r \end{bmatrix}^{\mathrm{T}}$ which is the reference position that is required to reach by the end-effector of the robotic arm and $\phi(\mathbf{q})$ is the position of the end-effector which is calculated using the forward kinematics equation (3.6). We define a Lyapunov function as follows [35]:

$$v(t) = \frac{1}{2}\mathbf{s}^{\mathrm{T}}\mathbf{s}. \tag{3.13}$$

Taking the time-derivative of (3.13) yields:

$$\dot{v}(t) = -\mathbf{s}^{\mathrm{T}}\dot{\mathbf{s}} = -\mathbf{s}^{\mathrm{T}}\mathbf{J}(\mathbf{q})\dot{\mathbf{q}}. \tag{3.14}$$

As taking time-derivative of (3.12) gives $\dot{\mathbf{s}} = -\dot{\phi}(\mathbf{q})$ (because $\dot{\mathbf{x}_\mathbf{r}} = 0$ as $\mathbf{x_r}$ is constant). Multiplying both sides of (3.10) by $\mathbf{J}(\mathbf{q})$ yields:

$$\mathbf{J}(\mathbf{q})\dot{\mathbf{q}} = \mathbf{K}\mathbf{s}. \tag{3.15}$$

Substituting (3.15) in (3.14) yields:

$$\dot{v}(t) = -\mathbf{s}^{\mathrm{T}}\mathbf{K}\mathbf{s}, \tag{3.16}$$

Therefore setting $\dot{\mathbf{q}} = \mathbf{J}^{-1}(\mathbf{q})\mathbf{K}\mathbf{s}$ as in (3.10), results in a negative-definite time-derivative of the Lyapunov function as $\dot{v}(t) = -\mathbf{s}^{\mathrm{T}}\mathbf{K}\mathbf{s} < 0$. This allows us to integrate (3.10) to solve for the generalized coordinates that achieves a desired position of the end-effector as shown in Fig. 3.2. By setting $\mathbf{K} = \begin{bmatrix} 10000 & 10000 & 10000 \end{bmatrix}^{\mathrm{T}}$, the error in the generalized coordinates resulting from the feedback stabilization method is approximately zero (error in range of 10^{-9}).

3.1.2 Modeling of the Microparticle

The equation of motion of a paramagnetic microparticle moving in a fluid with low Reynolds number under the influence of the magnetic field gradients

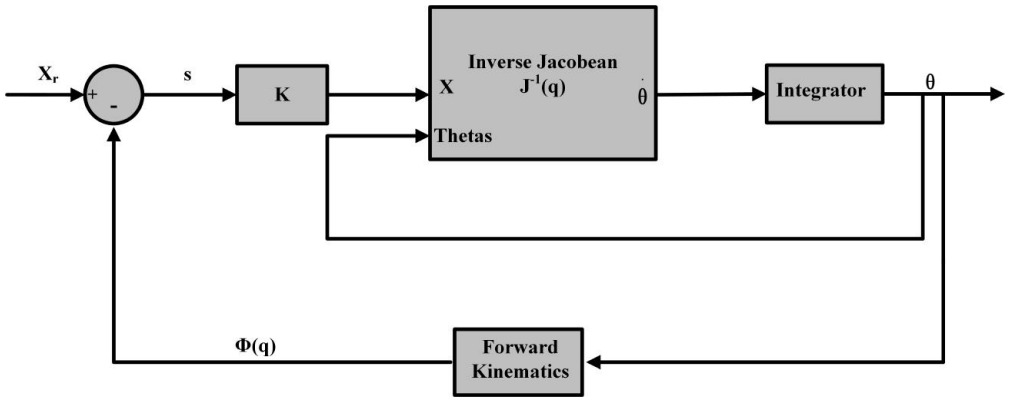

FIGURE 3.2: Inverse Kinematics of the robotic arm using feedback stabilization method. $\mathbf{x_r}$ is the required reference position of the end-effector, $\mathbf{K}$ is a positive-definite matrix, $\mathbf{q}$ is a vector of generalized coordinates, θ_k are the thetas of the revolute joints of the robotic arm for $k = 1, \ldots, 4$, $\phi(\mathbf{q})$ is the position of the end-effector which is calculated using the forward kinematics and $\mathbf{s}$ is the error calculated between the $\mathbf{x_r}$ and $\phi(\mathbf{q})$.

is given by:

$$\nabla\left(\mathbf{m}(\mathbf{P})\cdot\mathbf{B}(\mathbf{P})\right)+6\pi\eta r_{\mathrm{p}}\dot{\mathbf{P}}+V(\rho_{\mathrm{b}}-\rho_{\mathrm{f}})\mathbf{g}=0, \tag{3.17}$$

where $\mathbf{m}(\mathbf{P})$ and $\mathbf{B}(\mathbf{P})$ are the magnetic dipole moment of the microparticle and the induced magnetic field at a point $\mathbf{P}$, respectively. Further, η and r_{p} are the fluid dynamic viscosity and radius of the microparticle ($r_{\mathrm{p}}=50\ \mu$m), respectively. Furthermore, V and ρ_{b} are the volume and density of the microparticle (1.4×10^{3} kg/m^{3}) respectively, ρ_{f} is the density of the fluid where the microparticle is placed (the fluid used in this work is water whose $\rho_{\mathrm{f}}=1000$ kg/m^{3}) and $\mathbf{g}$ is the acceleration due to gravity [36]. Equation (3.17) shows the forces exerted on the microparticles which are: the magnetic force ($\nabla\left(\mathbf{m}(\mathbf{P})\cdot\mathbf{B}(\mathbf{P})\right)$) exerted on the microparticles by a permanent magnet or by an electromagnetic coil, the drag force ($6\pi\eta r_{\mathrm{p}}\dot{\mathbf{P}}$) and buoyancy force ($V\rho_{\mathrm{f}}\mathbf{g}$) exerted on the microparticles by the fluid. While the forces exerted by the microparticles on the fluid are: the weight of the microparticles ($V\rho_{\mathrm{b}}\mathbf{g}$).

The magnetic force in (3.17) is generated using a permanent magnet or an electromagnetic coil that can be attached to the end-effector of a robotic. Motion control of the microparticle is achieved by controlling the generalized coordinates at the joint space to orient the magnetic field gradients of the permanent magnetic and electromagnetic coil towards a reference position using equation (3.10).

3.2 Microparticles Tracking and Pixels Calibration

The feedback in the magnetic-based robotic system is given by a digital microscope, the microscope provides a live stream video of the microparticle while it is inside the glass tube containing water. An object tracking software is implemented using the computer vision system toolbox in simulink. This software tracks and gives the position of the microparticle in the x- and z-directions in pixels. The size of the image produced from the microscope is 640 pixels along the x-direction and 480 pixels along the z-direction. Calibration is done to convert the position of the microparticle which is given in pixels to cm by taking an image to a 1 cm in the ruler by the microscope after tuning its focus and then counting how many pixels in this 1 cm. It is found that a 1 cm is equivalent to 491 pixels.

In this system, there are more than one frame as shown in Fig. 3.1, robotic arm frames, digital microscope frames (one in the center of the microscope and the other is at the upper-left corner of the microscope) and the object (microparticles) frame. The transformation matrix between any two different frames (F_1 and F_2) are calculated using equation (3.18) which represent the rotation about the (x, y and z)-axes and translation in space across the (x, y

and z)-axes:

$$^{\mathbf{F_1}}\mathbf{T}_{\mathbf{F_2}} = \begin{bmatrix} C\psi C\theta & C\psi S\theta S\phi - S\psi C\phi & C\psi S\theta C\phi + S\psi S\phi & d_x \\ S\psi C\theta & S\phi S\theta S\phi + C\psi C\phi & S\psi S\theta C\phi - C\psi S\phi & d_y \\ -S\theta & C\theta S\phi & C\theta C\phi & d_z \\ 0 & 0 & 0 & 1 \end{bmatrix}, \quad (3.18)$$

where ϕ is the angle obtained by rotating around the x-axis of F_2 till the x-axis of F_1, θ is the angle obtained by rotating around the y-axis of F_2 till the y-axis of F_1, ψ is the angle obtained by rotating around the z-axis of F_2 till the z-axis of F_1, d_x is the distance obtained by translating along the x-axis of F_1 till the x-axis of F_2, d_y is the distance obtained by translating along the y-axis of F_1 till the y-axis of F_2 and d_z is the distance obtained by translating along the z-axis of F_1 till the z-axis of F_2.

$^{\mathbf{CS}}\mathbf{T}_{\mathbf{Object}}$ is the transformation matrix which relates the frame of the upper-left edge of the microscope image (CS) to the frame of the microparticles swimming inside the tube (Object):

$$^{\mathbf{CS}}\mathbf{T}_{\mathbf{Object}} = \begin{bmatrix} 1 & 0 & 0 & Q_x \\ 0 & 1 & 0 & -3 \\ 0 & 0 & 1 & Q_z \\ 0 & 0 & 0 & 1 \end{bmatrix}, \quad (3.19)$$

where Q_x is acquired by multiplying the position of the microparticle in the x-direction in pixels obtained from the object tracking software, by 1/491 (so

as to convert pixels to cm). Q_z is acquired by multiplying the position of the microparticle in the z-direction in pixels obtained from the object tracking software, by 1/491 (so as to convert pixels to cm). The two frames of the upper-left edge of the microscope (X_s, Y_s, Z_s) and the microparticle (X_{obj}, Y_{obj}, Z_{obj}), have the same orientation. There are displacements Q_x along the positive x-direction, 3 cm along the negative y-direction and Q_z along the positive z-direction.

$^{\mathbf{Rbase}}\mathbf{T_{CC}}$ is the transformation matrix which relates the frame of the base of the robotic arm (Rbase) to the frame of the center of the microscope (CC):

$$^{\mathbf{Rbase}}\mathbf{T_{CC}} = \begin{bmatrix} 1 & 0 & 0 & 0 \\ 0 & 1 & 0 & 26 \\ 0 & 0 & 1 & -1.5 \\ 0 & 0 & 0 & 1 \end{bmatrix}, \tag{3.20}$$

The two frames of the robotic arm base (X_0, Y_0, Z_0) and the center of the microscope (X_c, Y_c, Z_c), have the same orientation. The same displacement along x-direction and there are displacements 26 cm along the positive y-direction and 1.5 cm along the negative z-direction.

$^{\mathbf{CC}}\mathbf{T_{CS}}$ is the transformation matrix which relates the frame of the center of the microscope (CC) to the frame of the upper-left corner of the microscope

image (CS):

$$^{\mathbf{CC}}\mathbf{T}_{\mathbf{CS}} = \begin{bmatrix} -1 & 0 & 0 & K_x \\ 0 & 1 & 0 & 3 \\ 0 & 0 & -1 & K_z \\ 0 & 0 & 0 & 1 \end{bmatrix}, \tag{3.21}$$

where K_x is acquired by multiplying 320 pixels (which is the half the number of pixels in the x-direction), by 1/491 (so as to convert pixels to cm). K_z is acquired by multiplying 240 pixels (which is the half the number of pixels in the z-direction), by 1/491 (so as to convert pixels to cm). The two frames of the center of the microscope (X_c, Y_c, Z_c) and the upper-left edge of the microscope (X_s, Y_s, Z_s), are oriented by 180° around the y-axis. There are displacements K_x along the positive x-direction, 3 cm along the positive y-direction and K_z along the positive z-direction.

The world frame of the magnetic-based robotic system (X_0, Y_0, Z_0) is related to the microparticle swimming in the glass tube $(X_{obj}, Y_{obj}, Z_{obj})$ using the following equation:

$$^{\mathbf{Rbase}}\mathbf{T}_{\mathbf{Object}} = ^{\mathbf{Rbase}}\mathbf{T}_{\mathbf{CC}}\ ^{\mathbf{CC}}\mathbf{T}_{\mathbf{CS}}\ ^{\mathbf{CS}}\mathbf{T}_{\mathbf{Object}}, \tag{3.22}$$

where $^{\mathbf{Rbase}}\mathbf{T}_{\mathbf{Object}}$ is the transformation matrix of the actual position of the microparticle swimming inside the tube (Object) relative to the base of the robotic arm frame (Rbase).

3.3 Control of Microparticles using Magnetic-Based Robotic System

Controlling of the magnetic-based robotic system involves controlling the system using permanent magnet and controlling using electromagnetic coil.

3.3.1 Control using Permanent Magnet

Control of the magnetic force in (3.17) is achieved using the position and orientation of the end-effector of the robotic arm as shown in Fig. 3.3. It is

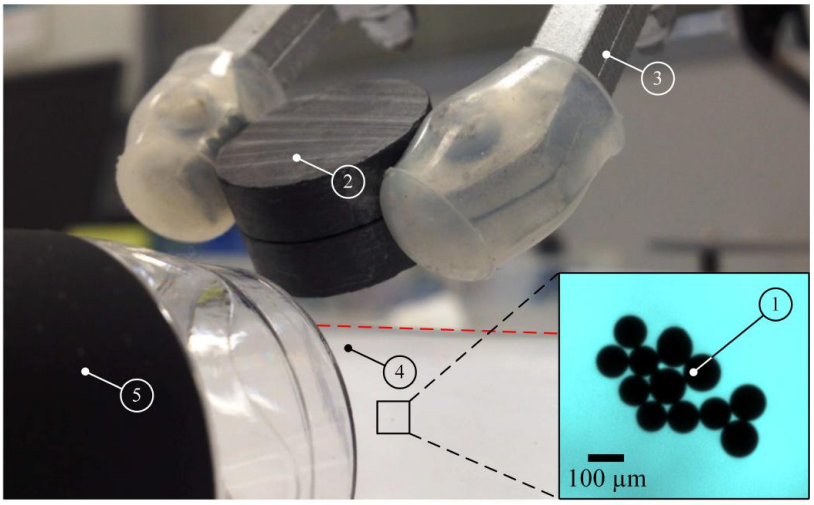

FIGURE 3.3: Motion control of paramagnetic microparticles ① using a permanent magnet ② and a robotic arm (not shown). The permanent magnet is fixed to the end-effector ③ of the robotic arm and the particles are contained inside a glass tube ④ that is filled with water. Closed-loop motion control of the microparticles is achieved using microscopic ⑤ feedback. The red-dashed line indicates the upper edge of the glass tube. The open-configuration of this magnetic-based robotic system allows us to control the motion of the microparticles throughout a relatively large workspace with a field of view of 10 mm×10 mm×10 mm. The maximum magnetic field of the permanent magnet is 85 mT.

clear from Fig. 3.4 that the microparticles (the red arrow indicates the microparticles)are contained in water inside a glass tube and their position ($\mathbf{P}$) is determined using a microscopic system and a feature tracking software. The control system positions the microparticles (based on the given reference position $\mathbf{P}_{\text{ref}}$) by controlling the position and orientation of the permeant magnet through the robotic arm. θ and $\mathbf{U}$ represent vectors of the generalized coordinates of the robotic arm and control inputs, respectively. The robotic arm changes the position of the end-effector, and hence controls the magnetic field gradient exerted on the microparticle. A proportional (P) magnetic force is devised as follows:

$$\nabla \left(\mathbf{m}(\mathbf{P}) \cdot \mathbf{B}(\mathbf{P}) \right) = \mathbf{K}_{\text{p}} \mathbf{e}, \tag{3.23}$$

where $\mathbf{K}_{\text{p}}$ is the proportional gain matrix. Further, $\mathbf{e}$ is the position error and is give by:

$$\mathbf{e} = \mathbf{P}_{\text{ref}} - \mathbf{P}. \tag{3.24}$$

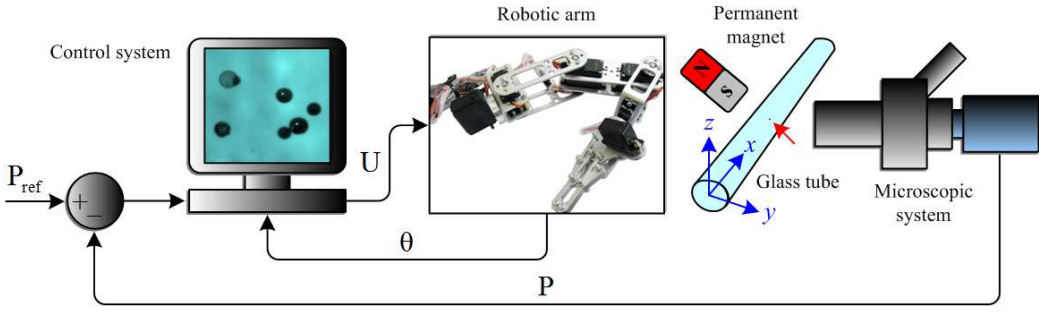

FIGURE 3.4: Closed-loop motion control of the position of a paramagnetic microparticle using the robotic arm holding the permanent magnet. The particles are contained in water inside a glass tube and their position ($\mathbf{P}$) is determined using a microscopic system and a feature tracking software. The control system positions the microparticles (based on the given reference position $\mathbf{P}_{\text{ref}}$) by controlling the position and orientation of the permeant magnet through the robotic arm. θ and $\mathbf{U}$ represent vectors of the generalized coordinates of the robotic arm and control inputs, respectively. The red arrow indicates the microparticles.

From(3.24), $\mathbf{P}_{\text{ref}}$ is a fixed reference position which is given to the closed-loop control as an input and $\mathbf{P}$ is the feedback position that is determined using the digital microscope. Substituting (3.24) in (3.23) yields the following equation:

$$\nabla \left(\mathbf{m}(\mathbf{P}) \cdot \mathbf{B}(\mathbf{P}) \right) = \mathbf{K}_{\text{p}} (\mathbf{P}_{\text{ref}} - \mathbf{P}), \tag{3.25}$$

Then by substituting (3.25) in (3.17) gives the following error dynamics equation:

$$\mathbf{\Lambda} \mathbf{K}_{\text{P}} \mathbf{e} + \mathbf{\Lambda} V (\rho_{\text{b}} - \rho_{\text{f}}) \mathbf{g} + \dot{\mathbf{P}} = 0, \tag{3.26}$$

where $\mathbf{\Lambda}$ is given by:

$$\mathbf{\Lambda} = \left(6\pi\eta r_{\text{p}} \mathbf{\Pi} \right)^{-1}. \tag{3.27}$$

Based on (3.26), the control gain matrices must be selected such that the matrix $\mathbf{\Lambda} \mathbf{K}_{\text{P}}$ is positive-definite. The magnetic field gradients ($\frac{\partial \mathbf{B}(\mathbf{P})}{\partial x}$, $\frac{\partial \mathbf{B}(\mathbf{P})}{\partial y}$, and $\frac{\partial \mathbf{B}(\mathbf{P})}{\partial z}$) that are required to pull the microparticle towards a reference position ($\mathbf{P}_{\text{ref}}$) can be determined by solving (3.23). These gradients can be achieved by controlling the position of the end-effector of the robotic arm with respect to the microparticle and this is done by keeping a constant distance between them. Thus, keeping constant magnetic field gradients on the microparticle. The magnetic field gradients generated from permanent magnet (shown in the last chapter in 2.1) are relatively large enough to overcome the gravitational and drag forces.

In order to control the position of the microparticle in the x- and z-directions, equation (3.10) is used to solve for the generalized coordinates (calculating

the values of the angles of the motors attached to each link of the robotic arm) that achieves a desired position of the end-effector holding the permanent magnet with respect to the position of the microparticles. This position direct the magnetic field gradients towards the reference position. This level of control allows the microparticles to be suspended inside the glass tube and move towards the reference positions under the influence of a constant magnetic field gradient. The gradient is kept constant by the closed-loop control on the joints of the robotic arm based on the relative position between the microparticle and the permanent magnet.

3.3.2 Control using Electromagnetic Coil

An electromagnetic coil is attached to the end-effector of the robotic arm. Therefore, The magnitude of the magnetic field gradient is controlled by using an electromagnetic coil instead of the permanent magnet. Thus, the equation of motion (3.17) is given by:

$$\nabla \left(\mathbf{m}(\mathbf{P}) \cdot \widetilde{\mathbf{B}}(\mathbf{P}) I \right) + 6\pi\eta r_{\mathrm{p}} \dot{\mathbf{P}} + V(\rho_{\mathrm{b}} - \rho_{\mathrm{f}})\mathbf{g} = 0, \tag{3.28}$$

where I and $\widetilde{\mathbf{B}}(\mathbf{P})$ are the current input to the electromagnetic coil and the magnetic field-current map, respectively. Unlike the motion control using the robotic arm and the permanent magnet, (3.28) indicates that using an electromagnetic coil with the robotic arm allows us to change the magnitude of the pulling magnetic force that is exerted on the microparticles. However, the direction of this pulling magnetic force can only be controlled using the posi-

tion and orientation of the end-effector of the robotic arm. This means that by using the electromagnetic coil increases the degrees of freedom of the magnetic-based robotic system, as the position of the microparticle is controlled using the position of the end-effector and the current of the electromagnetic coil. The magnetic field gradients generated from the electromagnetic coil (shown in the last chapter in 2.2) are relatively large enough to overcome the gravitational and drag forces. Fig. 3.5 shows the configuration of the closed-loop control system of the microparticles using the electromagnetic coil. It is obvious from the figure that the microparticles (the red arrow indicates the microparticles) are contained in water inside a glass tube and their position ($\mathbf{P}$) is determined using a microscopic system and a feature tracking algorithm. The control system positions the microparticles (based on the given reference position $\mathbf{P}_{\text{ref}}$) by controlling the position and orientation of the coil through the robotic arm

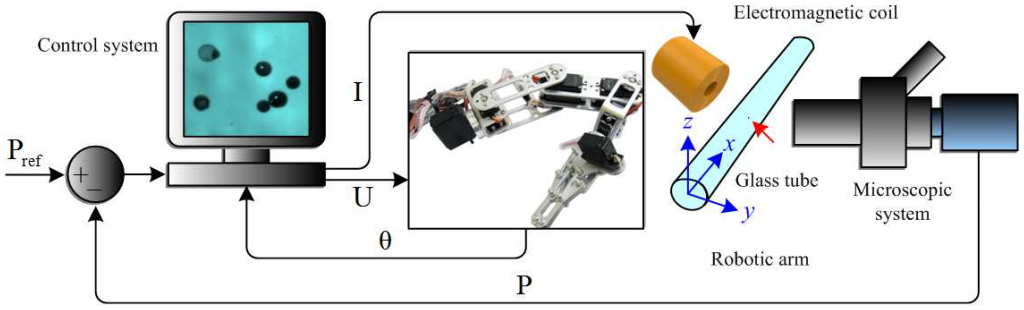

FIGURE 3.5: Closed-loop motion control of the position of a paramagnetic microparticle using the robotic arm holding the electromagnetic coil. The particles are contained in water inside a glass tube and their position ($\mathbf{P}$) is determined using a microscopic system and a feature tracking software. The control system positions the microparticles (based on the given reference position $\mathbf{P}_{\text{ref}}$) by controlling the position and orientation of the coil through the robotic arm and its current input ($\mathbf{I}$). θ and $\mathbf{U}$ represent vectors of the generalized coordinates of the robotic arm and control inputs, respectively. The red arrow indicates the microparticles.

and its current input (**I**). θ and **U** represent vectors of the generalized coordinates of the robotic arm and control inputs, respectively.

The position of the microparticles is determined using the microscopic system and used to determine the position and orientation of the electromagnetic coil with respect to the microparticles. In addition, the input current of the electromagnetic coil is used to change the magnitude of the pulling magnetic force towards the reference position. The current (I) of the electromagnetic coil is used to suspend the microparticle in the z-direction (z) and makes it reach the reference z-position (z_r). While The x-position of the microparticle is controlled using the position of the end-effector (x) to reach to the reference x-position (x_r). The end-effector of the robotic arm is controlled using P controller as in subsection (3.3.1). However the current (I) of the electromagnetic coil is controlled using proportional (P), proportional-derivative (PD) and proportional-integral-derivative (PID) controllers.

3.3.2.1 Control using P Controller

The current (I) of the electromagnetic coil is controlled using P controller. The equation of motion (3.28) is used to derive a similar error dynamics equation to (3.26) when a P magnetic force input is applied using (3.23).

3.3.2.2 Control using PD Controller

The current (I) of the electromagnetic coil is controlled using PD controller. A PD magnetic force is devised as follows:

$$\nabla \left(\mathbf{m}(\mathbf{P}) \cdot \widetilde{\mathbf{B}}(\mathbf{P}) I \right) = \mathbf{K}_{\mathrm{p}} \mathbf{e} + \mathbf{K}_{\mathrm{D}} \dot{\mathbf{e}}, \tag{3.29}$$

where $\mathbf{K}_{\mathrm{D}}$ is the derivative gain matrix. Further, $\dot{\mathbf{e}}$ is the velocity error. The velocity error is calculated by taking the derivative of the position error given in (3.24) which gives:

$$\dot{\mathbf{e}} = -\dot{\mathbf{P}}. \tag{3.30}$$

From(3.30), $\dot{\mathbf{P}}_{\mathrm{ref}}$=0 as $\mathbf{P}_{\mathrm{ref}}$ is a fixed reference position which is given to the closed-loop control. Substituting (3.30) and (3.24) in (3.29) yields the following equation:

$$\nabla \left(\mathbf{m}(\mathbf{P}) \cdot \widetilde{\mathbf{B}}(\mathbf{P}) I \right) = \mathbf{K}_{\mathrm{p}} (\mathbf{P}_{\mathrm{ref}} - \mathbf{P}) - \mathbf{K}_{\mathrm{D}} \dot{\mathbf{P}}, \tag{3.31}$$

Then by substituting (3.31) in (3.17) gives the following error dynamics equation:

$$\mathbf{\Gamma K}_{\mathrm{P}} \mathbf{e} + \mathbf{\Gamma} V (\rho_{\mathrm{b}} - \rho_{\mathrm{f}}) \mathbf{g} - \dot{\mathbf{e}} = 0, \tag{3.32}$$

where $\mathbf{\Gamma}$ is given by:

$$\mathbf{\Gamma} = \left(-\mathbf{K}_{\mathrm{D}} + 6\pi\eta r_{\mathrm{p}} \mathbf{\Pi} \right)^{-1}. \tag{3.33}$$

The control gain matrices shown in (3.32) must be selected such that the matrix $\mathbf{\Gamma K}_{\mathrm{P}}$ is positive-definite.

3.3.2.3 Control using PID Controller

The current (I) of the electromagnetic coil is controlled using PID controller. A PID magnetic force is devised as follows:

$$\nabla \left(\mathbf{m}(\mathbf{P}) \cdot \widetilde{\mathbf{B}}(\mathbf{P}) I \right) = \mathbf{K}_{\mathrm{p}} \mathbf{e} + \mathbf{K}_{\mathrm{I}} \int \mathbf{e}\ \mathbf{dt} + \mathbf{K}_{\mathrm{D}} \dot{\mathbf{e}}, \tag{3.34}$$

where $\mathbf{K}_{\mathrm{I}}$ is the integral gain matrix and it is given by integrating (3.24) as shown:

$$\int \mathbf{e}\ \mathbf{dt} = \int (\mathbf{P}_{\mathrm{ref}} - \mathbf{P})\ dt. \tag{3.35}$$

Substituting with (3.35), (3.30) and (3.24) in (3.29) yields the following equation:

$$\nabla \left(\mathbf{m}(\mathbf{P}) \cdot \widetilde{\mathbf{B}}(\mathbf{P}) I \right) = \mathbf{K}_{\mathrm{p}} (\mathbf{P}_{\mathrm{ref}} - \mathbf{P}) + \mathbf{K}_{\mathrm{I}} \int (\mathbf{P}_{\mathrm{ref}} - \mathbf{P})\ dt - \mathbf{K}_{\mathrm{D}} \dot{\mathbf{P}}, \tag{3.36}$$

Then by substituting (3.36) and (3.33) in (3.17) gives the following error dynamics equation:

$$\mathbf{\Gamma K}_{\mathrm{P}} \mathbf{e} + \mathbf{\Gamma K}_{\mathrm{I}} \int \mathbf{e}\ \mathbf{dt} + \mathbf{\Gamma} V (\rho_{\mathrm{b}} - \rho_{\mathrm{f}}) \mathbf{g} - \dot{\mathbf{e}} = 0, \tag{3.37}$$

Based on (3.37), the control gain matrices must be selected such that the matrix $\mathbf{\Gamma K}_{\mathrm{P}}$ and $\mathbf{\Gamma K}_{\mathrm{I}}$ are positive-definite.

Chapter 4

Experimental Results

The experiments of the point-to-point motion control results are done using a magnetic-based robotic system. This system consists of a robotic arm that controls the position of a permanent magnet or an electromagnetic coil. In order to control the position of the microparticle in the glass tube.

4.1 Control using the Permanent Magnet

Point-to-point motion control of a paramagnetic microparticle is done by controlling the position of the permanent magnet such that the magnetic field gradients are oriented towards the reference position. Fig. 4.1 and Fig. 4.2 shows a representative motion control result of a microparticles towards a fixed reference position along x-axis and z-axis respectively, controlled by P controller (P=2). The position of the end-effector of the robotic arm is controlled using P controller only, as when PD and PID controllers are used the

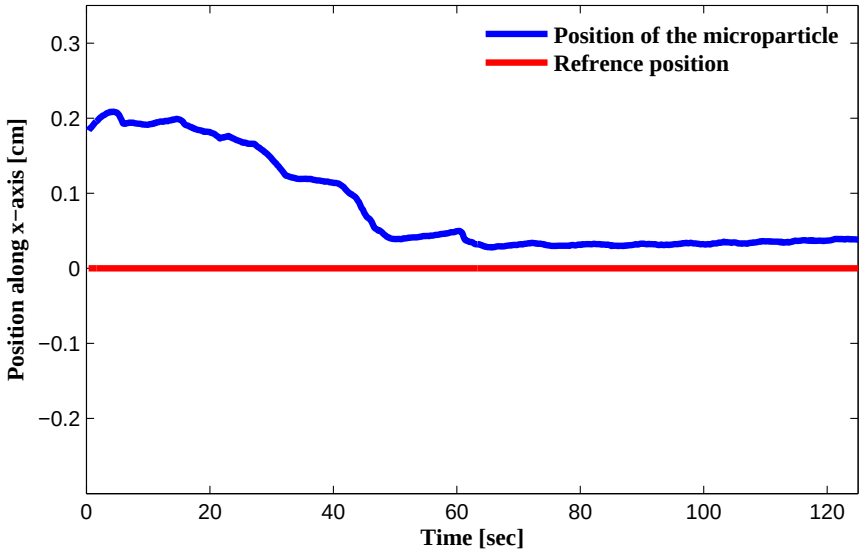

FIGURE 4.1: Closed-loop motion control of the position of a paramagnetic microparticle using a permanent magnet along x-axis. The average speed of the microparticle is 117 μm/s. The steady state error of the position of the microparticle in the x-direction is 400 μm.

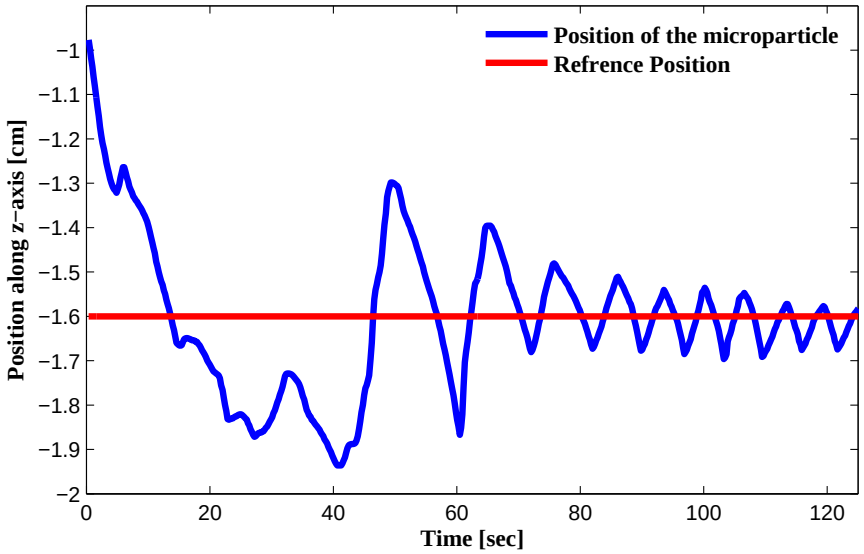

FIGURE 4.2: Closed-loop motion control of the position of a paramagnetic microparticle using a permanent magnet along z-axis. The average speed of the microparticle is 117 μm/s. The peak-to-peak amplitude of the suspended microparticle along the z-direction is 1.6 mm.

system is derived to instability. The microparticle is suspended and pulled towards the reference position at an average speed of 117 μm/s. In addition, it is observed that the peak-to-peak amplitude of the suspended microparticle along the z-direction of the reference position is 1.6 mm. Motion control of the microparticles can be enhanced by reducing the attractive magnetic force. This reduction is done by replacing the permanent magnet with an electromagnetic coil. This motion control trial is repeated 20 times and the average speed and position error in the x-direction in the steady-state are calculated to be 117 μm/s and 600 μm, respectively. The settling time of the microparticle is 70 sec.

It is concluded that the average position error in the steady-state is a little bit high as controlling the magnetic field in the case of using permanent magnet, depends only on the position of the end-effector of robotic arm. Thus, the steady state error is due to the low accuracy of the servo motors of the robotic arm (pointing accuracy of 0.5 degrees). It means that if the controller send an angle smaller than 0.5 degrees, the servo motors of the robotic arm will not be able to apply it.

4.2 Control using the Electromagnetic Coil

Closed-loop motion control of paramagnetic microparticles is achieved using an electromagnetic coil attached to the end-effector of the robotic arm. Controlling the position of the microparticle using the electromagnetic coil is done

by controlling the position and the current of the electromagnetic coil. The position of the electromagnetic coil is controlled to orient the magnetic field gradient towards the reference position using P controller. Also the current input to the electromagnetic coil is controlled to enhance the closed-loop control characteristics of the controlled microparticles, as opposed to the closed-loop control using the permanent magnet. Controlling the current of the electromagnetic coil, is implemented using three types of controllers:P, PD and PID controller.

4.2.1 Control using P Controller

Controlling the position of the microparticle is achieved by controlling the position of the electromagnetic coil by P controller where P equals to 2 and controlling the current of the electromagnetic coil by P controller where P equals to 100. Fig. 4.3 and Fig. 4.4 shows a representative closed-loop control of a microparticles along x-axis and z-axis respectively using P controller to control the current of the electromagnetic coil. The particles is controlled at an average speed of 48 μm/s, and the peak-to-peak amplitude along z-axis is calculated to be 1 mm, in the steady-state. This motion control is repeated 20 times and the average speed and position tracking error in the x-direction in the steady-state are calculated to be 48 μm/s and 100 μm, respectively. The settling time of the microparticle is 67 sec.

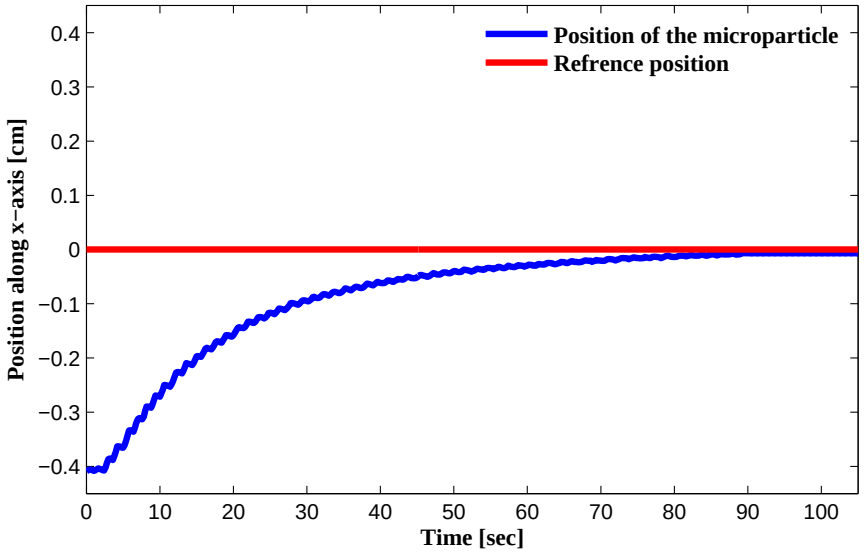

FIGURE 4.3: Closed-loop motion control of the position of a paramagnetic microparticle using an electromagnetic coil along x-axis. The average speed of the microparticle is 43 μm/s. The steady state error of the position of the microparticle in the x-direction is 70 μm.

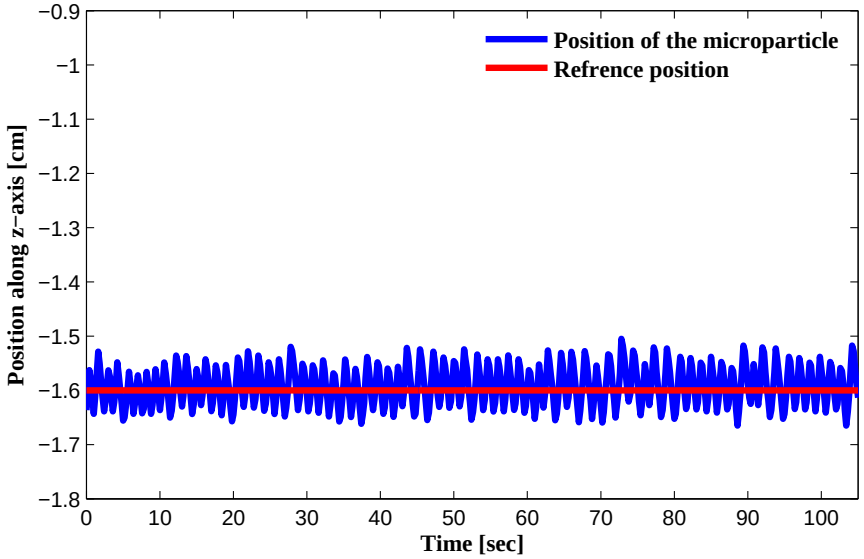

FIGURE 4.4: Closed-loop motion control of the position of a paramagnetic microparticle using an electromagnetic coil along z-axis. The average speed of the microparticle is 43 μm/s. The peak-to-peak amplitude of the suspended microparticle along the z-direction is 1 mm.

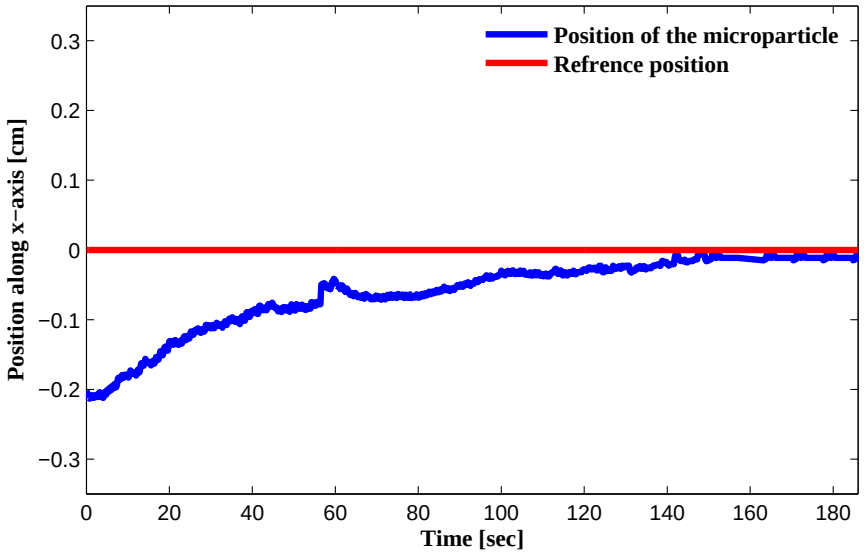

FIGURE 4.5: Closed-loop motion control of the position of a paramagnetic microparticle using an electromagnetic coil along x-axis. The average speed of the microparticle is 40 μm/s. The steady state error of the position of the microparticle in the x-direction is 108 μm.

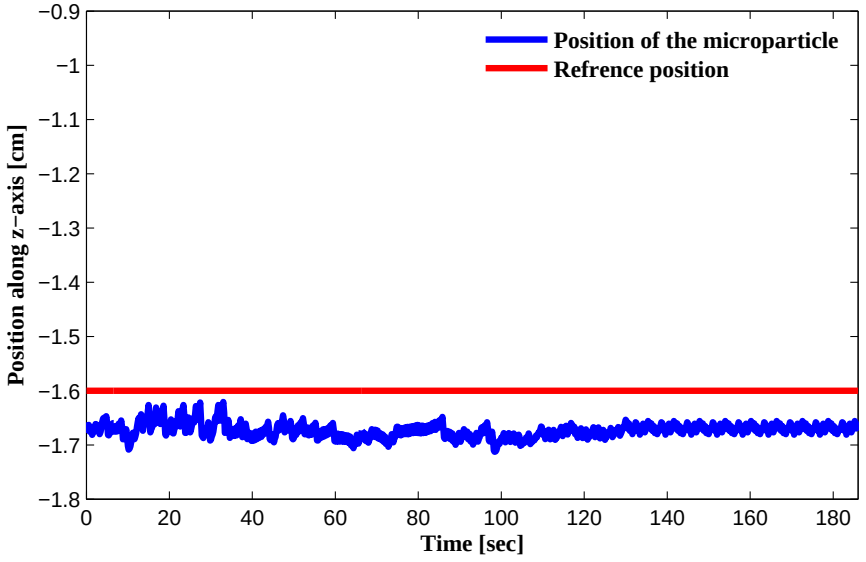

FIGURE 4.6: Closed-loop motion control of the position of a paramagnetic microparticle using an electromagnetic coil along z-axis. The average speed of the microparticle is 40 μm/s. The steady state error of the position of the microparticle in the z-direction is 686 μm. The peak-to-peak amplitude of the suspended microparticle along the z-direction is 0.1 mm.

4.2.2 Control using PD Controller

Closed-loop control of a microparticles along x-axis and z-axis using PD controller (P=100 and D=5) to control the current of the electromagnetic coil is shown in Fig. 4.5 and Fig. 4.6 respectively. The position of the electromagnetic coil is controlled using P controller where P equals to 2. The peak-to-peak amplitude of the suspended microparticle along the z-component of the reference position is 0.1 mm. The motion control experiment using PD controller is repeated 20 times. The average position steady state error in the x-direction and z-direction is 108 μm and 686 μm respectively. The average speed of the microparticle is 40 μm/s. The settling time of the microparticle is 140 sec.

4.2.3 Control using PID Controller

PID controller (P=100, I=3 and D=5) is used to control the current of the electromagnetic coil to control the position of the microparticle in the x-axis and z-axis as shown in Fig. 4.7 and Fig. 4.8 respectively. P controller (P=2) is used to control the position of the electromagnetic coil. The closed-loop control using PID controller is conducted 20 times. The average speed of the microparticle is 16 μm/s. The average position steady state error in the x-direction is 393 μm. The peak-to-peak amplitude of the suspended microparticle along the z-component of the reference position is 0.7 mm. The settling time of the microparticle is 400 sec.

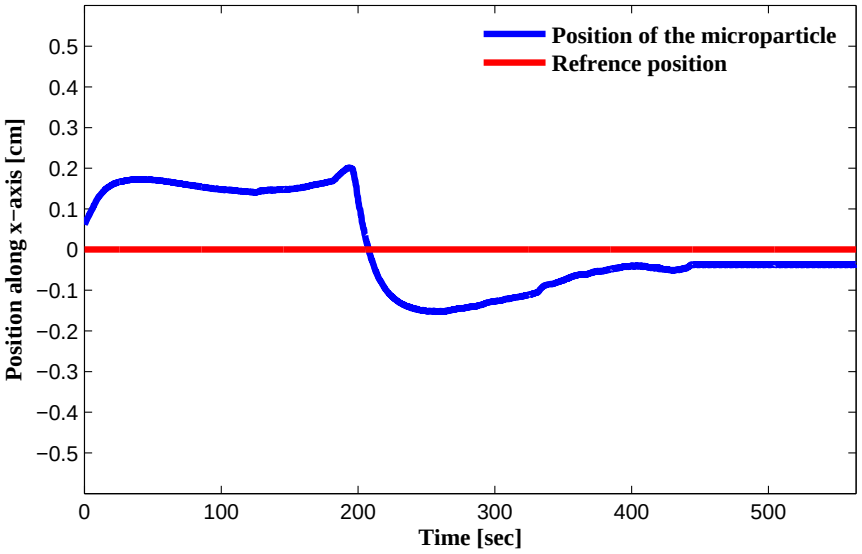

FIGURE 4.7: Closed-loop motion control of the position of a paramagnetic microparticle using an electromagnetic coil along x-axis. The average speed of the microparticle is 16 μm/s. The steady state error of the position of the microparticle in the x-direction is 393 μm.

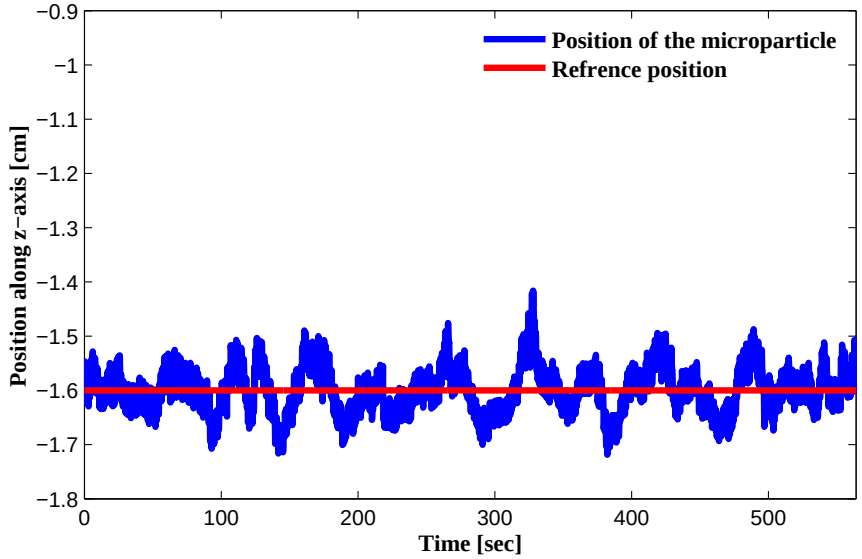

FIGURE 4.8: Closed-loop motion control of the position of a paramagnetic microparticle using an electromagnetic coil along z-axis. The average speed of the microparticle is 16 μm/s. The peak-to-peak amplitude of the suspended microparticle along the z-direction is 0.7 mm.

Chapter 5

Conclusions and Future Work

Magnetic-based robotic system is constructed including: robotic arm, glass tube that contains water, digital microscope and a permanent magnet or an electromagnetic coil. This system is used to control the position of the microparticle in the $x-$ and $z-$axes within the vicinity of 1 cm^2. The permanent magnet produces maximum magnetic field of 85 mT, and the electromagnetic coil produces maximum magnetic field of 7.5 mT at an input current of 0.6 A.

Point-to-point motion control of paramagnetic microparticles is achieved using a magnetic-based robotic system with open-configuration. This system allows us to suspend the microparticles along z-axis and achieve point-to-point motion control along a tube with a diameter of 40 mm. The experimental motion control trails shows that the permanent magnet and the robotic arm achieves motion control at an average speed of 117 μm/s, whereas the electromagnetic coils controlled by P controller and the robotic arm achieves average speed

of 48 μm/s. However, the electromagnetic coils and the robotic arm achieves higher positioning accuracy than the permanent magnet, in the steady-state. It is observed that the speed of the controlled microparticles using the electromagnetic coil (for maximum current of 0.6 A) and the robotic arm is 59% less than average speed of the microparticles driven using the permanent magnet and the robotic arm. The difference in the average speed is due to the maximum magnetic fields and field gradients that are generated using the permanent magnet and the electromagnetic coil, as shown in Figs. 2.3 and 2.4. It is obvious from the figures that magnetic fields generated by the permanent magnet is much higher than the magnetic fields generated by the electromagnetic coil. The closed-loop control characteristics (steady-state error and peak-to-peak amplitude) of the controlled microparticles using the electromagnetic coil and robotic arm are better than those of the permanent magnet and robotic arm. The average peak-to-peak amplitude of the controlled microparticles using the electromagnetic coil controlled by P controller is 38% less than that achieved by the permanent magnet. The position steady state error in case of using electromagnetic coil is 83% less than that of the permanent magnet. This difference is due to the current control input that allows the change in the magnitude of the pulling magnetic force by changing the magnitude of the magnetic fields gradient. This can not be done when the microparticles are controlled using the permanent magnets. Therefore, it is concluded that using electromagnetic coil in controlling the position of the microparticle is better than using permanent magnet.

Also it is observed that the position steady state error when controlling the

microparticle by electromagnetic coil using P controller in the x-direction is less than when it is controlled by PID controller by 75%, also it is less than when it is controlled using PD controller by 7%. The settling time when the microparticle is controlled by P controller is 110 sec, which is less than the settling time of PID controller whose value is 440 sec and less than PD controller whose value is 140 sec. Thus, P controller is preferable than PD and PID controllers in controlling the position of the microparticle using electromagnetic coil.

As part of future studies, the motion control system and experimental setup used in this thesis will be adapted to include physical constrains on the motion of the end-effector in the task-space. This would allow to control the motion of the microparticles inside the glass tube while following a trajectory in the task-space (to achieve axillary task, e.g., obstacle avoidance). In addition, the system will be modified by replacing the microscopic vision system with a clinical imagine modality, and the motion control will be done in the presence of a flowing stream of the fluid. Also, the control can be held in three dimensional space instead of the two dimensional space. Besides, The results can be enhanced by using non-linear control methods, when controlling the position of the end-effector of the robotic arm.

Appendix A

Microparticles

The position of the microparticles which are used to carry the drugs, is controlled using the magnetic fields that is generated from a permanent magnet and a robotic arm and the magnetic fields generated from an electromagnetic coil and a robotic arm. In order to reach the cells which contain the disease. The properties and specifications of these microparticles are attached in the following page.

TECHNICAL DATA SHEET

micromod Partikeltechnologie GmbH

Product code:	12-00-105
Product name:	PLA-M
Surface:	plain
Size:	100 µm
Solid content:	10 mg/ml
Composition:	magnetic poly(lactic acid) particles
Standard deviation:	)*
Shape:	spherical
Density:	1.3 g/ccm
Magnetization:	4.3 emu/g particles (H =1000 Oe)
Saturation magnetization:	> 6.6 emu/g particles (H > 10.000 Oe)
Stable in:	aqueous buffers pH > 4
Not stable in:	organic solvents, acidic solutions pH < 4
Product form:	suspension in water
Particles per ml:	1.5*10E4
Particles per mg:	1.5*10E3
Colour:	dark brown
Additional remarks:	Storage at 2 - 8°C for 6 months
TECHNOTES:	)* Size cut: 70 µm - 150 µm

Appendix B

Robotic Arm

The robotic arm consists of 6 servo motors, but it is modeled as 4 DOF robotic arm as the last servo motors are not used in our experiments (one of them is responsible for rotating the end-effector and the other one is responsible for opening and closing the gripper). These two servo motors are set to a certain angle and not changed throughout the experiments. The dimensions of the robotic arm is shown in Fig. 2.2. The specifications of the first three servo motors are found in the page while the specifications of the last servo motor is found in the page after.

Servo motor specifications and parameters as follows:

12KG metal gear of the servo motor:
Size: 40.4 * 19.8 * 36 mm
Weight: 48 g
Speed: 0.22 sec/60 °
Output Torque: 13 kg • cm

3.2kg servo motor:
Size: 39.5 x20.0x35.5mm
Weight: 41 g
Speed: 0.27 sec/60 °
Torque output: 3.2 kg • cm

3.2kg servo motor:
Size: 28 x14x29.8mm
Weight: 18 g
Speed: 0.13 sec/60 °
Torque output: 2.3 kg • cm

S06NF STD

Package:

One polybag one piece

Description:

56.0gwith torque 13.0kg-cm (6v) 13.5kg-cm (7.2V);wire: 30cm Metal Gear Servo.

Feature:

- Futaba, JR, Sanwa and Hitec compatible.

Important Notes:

- Specify the connector type when you purchase the servo.
- Refer to the figure when installing the servo accessories.
- For engine powered airplanes and boats, rubber must be used to reduce vibration.
- Please choose correct model for your application.
- Torque over-loaded will damage the servo's mechaniSM-.
- Keep the servo clean and away from dust, corrosive gas and humid air.

Specification

(Specifications are subjected to change without notice.)

Wire (cm)	Size (MM)					Weight		6V			7.2V		
								Speed	Torque		Speed	Torque	
	A	B	C	D	E	g	oz	sec/60°	kg-cm	oz-in	sec/60°	kg-cm	oz-in
30.0	40.4	20	37.6	48	10.0	56.0		0.18	13.0		0.16	13.5	

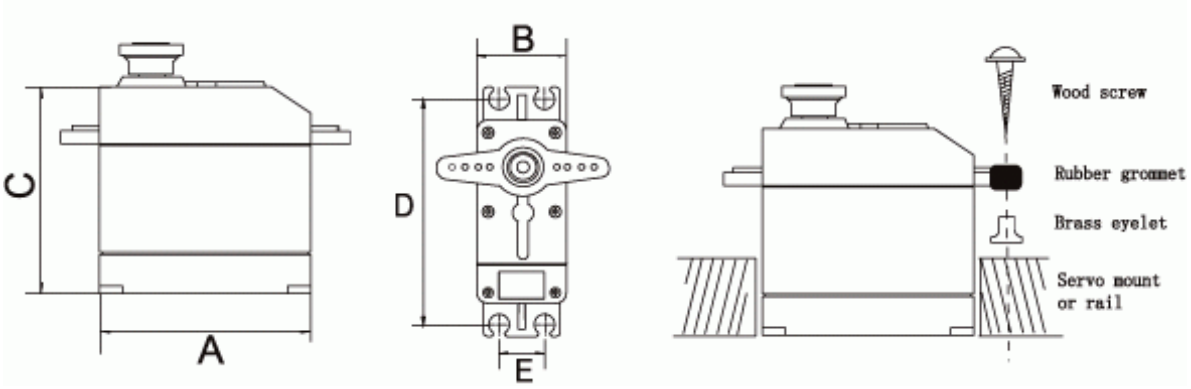

Appendix C

Digital Microscope

The digital microscope is used to provide the feedback in the magnetic-based robotic system. The microscope gives a live stream video and a feature tracking algorithm is used to track the position of the microparticle. It is connected to the computer via a USB 2.0 port. The parts and specifications of the digital microscope is found in the following two pages.

Parts Names

1.Snapshot button

2.Focus adjustment wheel

■ Computer System Requirements

- Win2000/XP/VISTA/WIN7&Mac10.5 and above
- P4 1.8 or above
- RAM: 256M
- Video Memory: 32M
- USB port: 2.0
- CD-ROM Drive

■ Technical Specifications

Image sensor	1.3 Mega Pixels (interpolated to 2M)
Still capture resolution	1600x1200 (2M), 1280x1024, 1024x960, 1024x768, 800x600, 640x480, 352x288, 320x240, 160x120
Video capture resolution	1600x1200 (2M), 1280x1024, 1024x960, 1024x768, 800x600, 640x480, 352x288, 320x240, 160x120
Focus Range	Manual focus from 10mm to 500mm
Frame Rate	Max 30f/s under 600 Lus Brightness
Magnification Ratio	20x to 200x
Video format	AVI
Photo format	JPEG or BMP
Light source	8 LED (adjustable by control wheel)
PC interface	USB2.0
Power source	5V DC from USB port
Operation system	Windows2000/XP/Vista/Win7/ Mac 10.5 and above
OSD language	English, German, Spanish, Korean, French, Russian
Bundle software	MicroCapture
Size	110mm (L) x 33mm (R)

Appendix D

Coil Driver

The driver is connected to the following signals: a power supply (4.5 V-12 V), a control signal (5 V) coming from the control broad like Arduino which is used in this work and a ground signal. Its output signal is connected to any coil (motor) which requires voltage input (4.5 V-12 V) and current of 4.5 A. It can be connected to 4 coils (motors) at the same time. The specifications and details of the driver used is found in the following two pages.

Designed originally for the Rover 5 chassis this driver PCB is ideal for any small robot using either Omni or Mecanum wheels. Current sensing for each motor allows the processor to determine if a motor has stalled or is under excessive load.

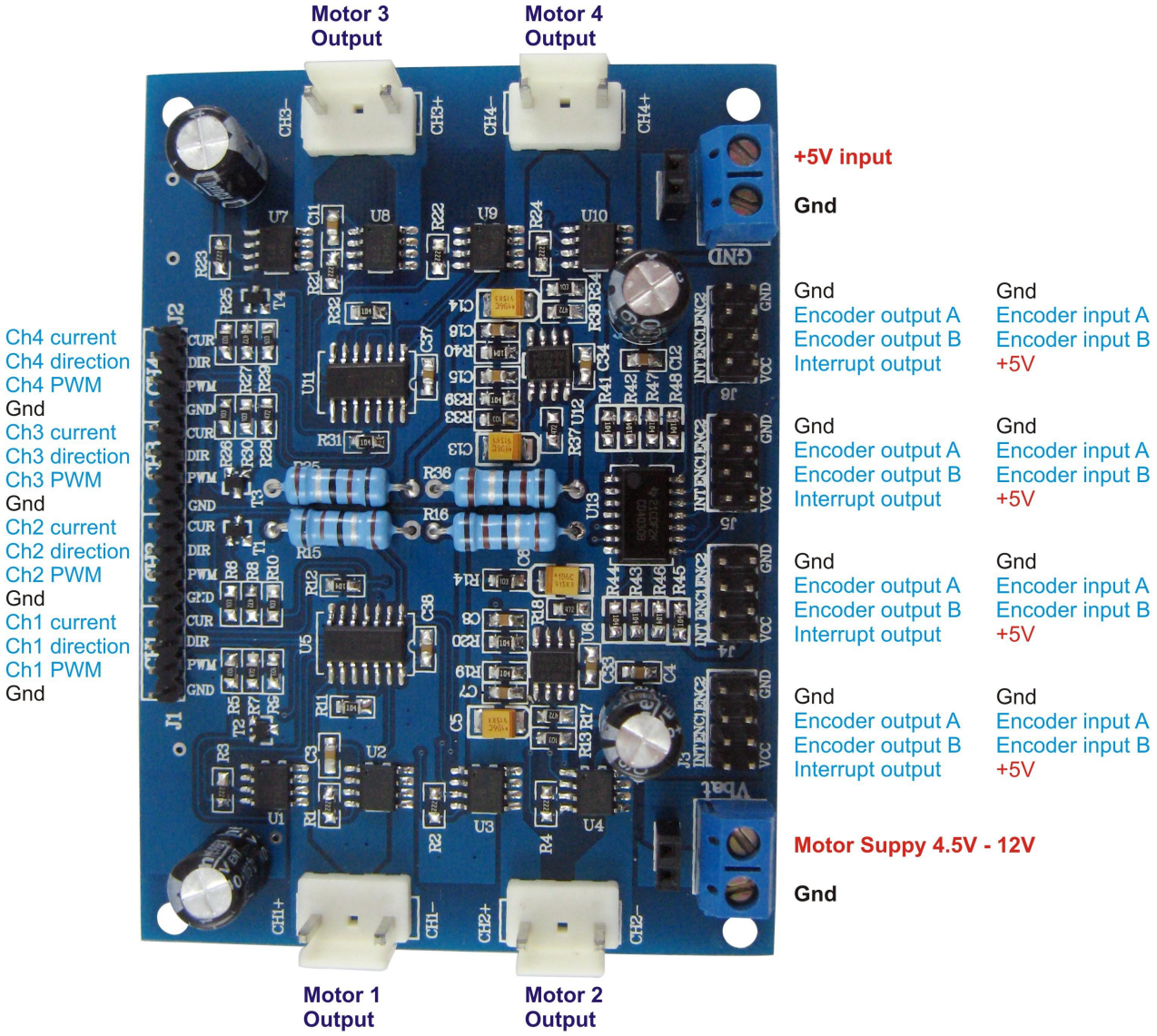

Features include:

- 4x low resistance FET “H” bridges.
- Each channel rated for 4A stall current.
- Easy to use control logic.
- Current monitoring for each channel.
- Quadrature encoder mixing circuitry.

Power connectors:
The PCB has two power connectors. One is +5V for logic (Vcc) and one for the motor power supply. The motor power supply should not be connected without first connecting the +5V for logic. This device is rated for a maximum motor supply voltage of 12V. Exceeding this voltage may permanently damage the device.

The encoder mixing circuit:
Unlike most motor controllers this PCB includes 4 mixing circuits for use with up to 4 quadrature encoders. The mixing circuit takes the 2 inputs from a quadrature encoder and mixes them into a single output. Note that the interrupt output changes state when either input changes.

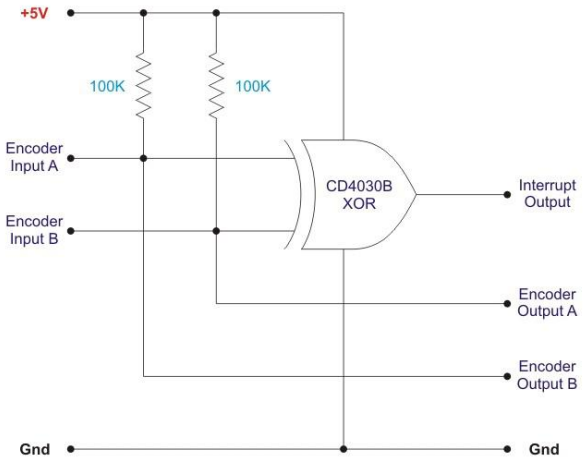

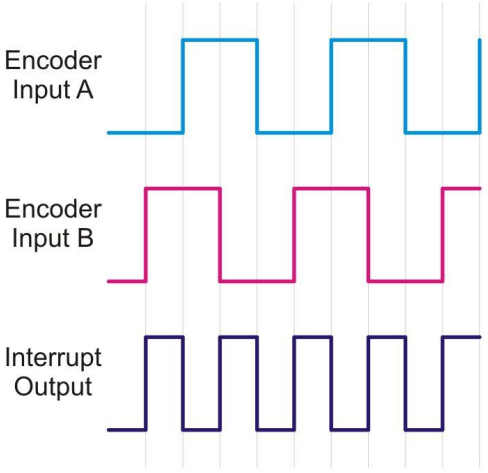

This allows a single interrupt pin to monitor both inputs of a quadrature encoder. Because the interrupt output is twice the frequency of either input it also allows speed and distance to be measured with twice the resolution.

Current output:
Each channel has a current sensing circuit. The output of this circuit is approximately 1V for each amp the motor draws (5V maximum). This output can be connected directly to the analog input of any 5V micro controller.

Control logic:
The built in control logic allows each motor to be controlled by 2 pins. Driving the **direction** pin high or low will cause the motor to run forward or reverse. The **PWM** pin is used to control the motor speed. When this pin is low, the motor is off. When this pin is high the motor is at full power. To vary the speed of the motor this pin must be Pulse Width Modulated.

Motor output:
Each channel has a motor output socket. Connect any 4.5V –12V DC motor with a stall current of less than 4.5A to these pins. Exceeding 4.5A on these pins may permanently damage this device.

Bibliography

[1] P. M. Devlin, "Brachytherapy: Applications and Techniques," *Lippincott Williams and Wilkins*, pp. 448, Philadelphia, 2007.

[2] B. J. Nelson, I. K. Kaliakatsos, and J. J. Abbott, "Microrobots for minimally invasive medicine," *Annual Review of Biomedical Engineering*, vol. 12, pp. 55-85, 2010.

[3] H. Zhang, D.W. Hutmacher, F. Chollet, A-N Poo, and E. Burdet, "Microrobotics and MEMS-based fabrication techniques for scaffold-based tissue engineering," *Macromol. Biosci.*, vol. 5, no. 6, pp. 477-89, 2005.

[4] R. Siegel, D. Naishadham, and A. Jemal, "Cancer statistics," *CA: A Cancer Journal for Clinicians*, vol. 62, no. 1, pp. 10-29, 2012.

[5] Q. A. Pankhurst, J. Connolly, S. K. Jones, and J. Dobson, "Applications of magnetic nanoparticles in biomedicine," *Journal of Physics*, vol. 36, no. 13, pp. 167-181, 2003.

[6] J. Weizenecker, B. Gleich, J. Rahmer, H. Dahnke, and J. Borgert, "Three-dimensional real-time in *vivo* magnetic particle imaging," *Physics in Medicine and Biology*, vol. 54, no. 5, pp. 1-10, 2009.

[7] R. Sinha, G. J. Kim, S. Nie, and D. M. Shin, "Nanotechnology in cancer therapeutics: bioconjugated nanoparticles for drug delivery," *Molecular Cancer Therapeutics*, vol. 5, no. 8, pp. 1909-1917, 2006.

[8] J.-B. Mathieu and S. Martel, "Steering of aggregatring magnetic microparticles using propulsion gradient coils in an MRI scanner," *Magnetic Resonance Medicine*, vol. 63, no. 5, pp. 1336-1345, 2010.

[9] I. S. M. Khalil, J. D. Keuning, L. Abelmann, and S. Misra, "Wireless magnetic-based control of paramagnetic microparticles," in *Proceedings of the IEEE RAS/EMBS International Conference on Biomedical Robotics and Biomechatronics (BioRob)*, pp. 460-466, Rome, Italy, 2012.

[10] J.-B. Mathieu and S. Martel, "Magnetic steering of iron oxide microparticles using proulsion gradient coils in MRI," in *Proceedings of the International Conference of the IEEE Engineering in Medicine and Biology Society (EMBS)*, pp. 472-475, New York City, USA, 2006.

[11] S. Martel, O. Felfoul, J.-B. Mathieu, A. Chanu, S. Tamaz, M. Mohammadi, M. Mankiewicz, and N. Tabatabaei, "MRI-based medical nanorobotic platform for the control of magnetic nanoparticles and flagellated bacteria for target interventions in human capillaries," *The International Journal of Robotics Research*, vol. 28, no. 9, pp. 1169-1182, 2009.

[12] M. P. Kummer, J. J. Abbott, B. E. Kartochvil, R. Borer, A. Sengul, and B. J. Nelson, "OctoMag: an electromagnetic system for 5-DOF wireless micromanipulation," *IEEE Transactions on Robotics*, vol. 26, no. 6,

pp. 1006-1017, 2010.

[13] B. E. Kratochvil, M. P. Kummer, S. Erni, R. Borer, D. R. Frutiger, S. Schüurle, and B. J. Nelson, "MiniMag: a hemispherical electromagnetic system for 5-DOF wireless micromanipulation," *Proceeding of the 12th International Symposium on Experimental Robotics*, New Delhi, India, 2010.

[14] S. Martel, J-B. Mathieu, O. Felfoul, H. Macicior, G. Beaudoin, G. Soulez, and L′H. Yahia, "Adapting MRI systems to propel and guide microdevices in the human blood circulatory system", in the *proceedings of the 26th Annual International Conference of the IEEE Engineering in Medicine and Biology Society*, pp. 1044-1047, 2004.

[15] M. S. Grady, M. A Howard III, J. A. Molloy, R. C. Ritter, E. G. Quate, and G. T. Gillies, "Nonlinear magnetic stereotaxis: three-dimensional, in vivo remote magnetic manipulation of a small object in canine brain," *International Scientific Journal Medical Physics*, vol. 17, no. 3, pp. 405-15, 1990.

[16] K. B. Yesin, K. Vollmers, and B. J. Nelson, "Modeling and control of untethered biomicrorobots in a fluidic environment using electromagnetic fields," *International Journal of Robotics Research*, vol. 25, no. 5-6, pp. 527-36, 2006.

[17] D. C. Meeker, E. H. Maslen, R. C. Ritter, and F. M. Creighton, "Optimal realization of arbitrary forces in a magnetic stereotaxis system," *IEEE Transactions on Magnetics*, vol. 32, no. 2, pp. 320-28, 1996.

[18] J. J. Abbott, K. E. Peyer, L. Dong, and B. Nelson, "*How should microrobots swim?*" *The International Journal of Robotics Research*, vol. 28, no. 11-12, pp. 1434-1447, 2009.

[19] L. Zhang, J. J. Abbott, L. X. Dong, B. E. Kratochvil, D. Bell, and B. J. Nelson, "Artificial bacterial flagella: fabrication and magnetic control," *Applied Physics Letters*, vol. 94, no. 6, pp. 064107, 2009.

[20] S. Sudo, S. Segawa, and T. Honda, "Magnetic swimming mechanism in a viscous liquid," *Journal of Intelligent Material Systems and Structures*, vol. 17, pp. 729-736, 2006.

[21] S. Guo, Q. Pan, and M. B. Khamesee, "Development of a novel type of microrobot for biomedical application," *Microsystem Technologies*, vol. 14, no. 307-314, 2008.

[22] I. S. M. Khalil, P. Ferreira, R. Eleutério,C. L. de Korte and S. Misra, "Magnetic-based closed-loop of paramagnetic microparticles using ultrasound feedback," in *Proceedings of the IEEE International Conference on Robotics and Automation (ICRA)*, pp. 3807-3812, Hong Kong, China, 2014.

[23] I. S. M. Khalil, J. D. Keuning, L. Abelmann, and S. Misra, "Wireless magnetic-based control of paramagnetic microparticles," in *Proceedings of the IEEE RAS/EMBS International Conference on Biomedical Robotics and Biomechatronics (BioRob)*, pp. 460-466, Rome, Italy, 2012.

[24] M. Evertsson, M. Cinthio, S. Fredriksson, F. Olsson, H. W. Persson, and T. Jansson, "Frequency- and phase-sensitive magnetomotive ultrasound

imaging of superparamagnetic iron oxide nanoparticles," in *IEEE Transcation on Ultrasonics, Ferroelectrics, and Frequency Control*, vol. 60, no. 3, pp. 481-491, 2013.

[25] S. Floyd, C. Pawashe, and M. Sitti, "Two-dimensional contact and non-contact micromanipulation in liquid using an untethered mobile magnetic microrobot," in *IEEE Transcation on Robotics*, vol. 25, no. 6, pp. 1332-1342, 2009.

[26] T. W. R. Fountain, P. V. Kailat, J. J. Abbott, "Wireless control of magnetic helical microrobots using a rotating-permanent-magnet manipulator", Robotics and Automation (ICRA), 2010 IEEE International Conference, pp. 576-581, 2010.

[27] A. W. Mahoney, D. L. Cowan, K. M. Miller, and J. J. Abbott, "Control of untethered magnetically actuated tools using a rotating permanent magnet in any position," in *Proceedings of the IEEE International Conference on Robotics and Automation (ICRA)*, pp. 3375-3380, Minnesota, USA, 2012.

[28] A. W. Mahoney and J. J. Abbott, "Control of untethered magnetically actuated tools with localization uncertainty using a rotating permanent magnet," in *Proceedings of the IEEE RAS/EMBS International Conference on Biomedical Robotics and Biomechatronics (BioRob)*, pp. 1632-1637, Rome, Italy, 2012.

[29] K. E. Peyer, L. Zhang, B. J. Nelson, "Bio-inspired magnetic swimming microrobots for biomedical applications", Nanoscale, vol. 5, no. 4, pp. 1259-1272, 2012.

[30] D. J. Bell, S. Leutenegger, K. M. Hammar, L. X. Dong, B. J. Nelson, "Flagella-like propulsion for microrobots using a magnetic nanocoil and a rotating electromagnetic field", in *Proceedings of the IEEE International Conference on Robotics and Automation (ICRA)*, pp. 1128-1133, 2007.

[31] J. Wang and W. Gao, "*Nano/Microscale motors: biomedical opportunities and challenges* " ACS Nano, vol. 6, no. 7, pp. 5745-5751, 2012.

[32] A. W. Mahoney and J. J. Abbott, "Managing magnetic force applied to a magnetic device by a rotating dipole field," *Applied Physics Letters*, vol. 99, no. 13, 2011.

[33] J. Weizenecker, B. Gleich, J. Rahmer, H. Dahnke, and J. Borgert, "Three-dimensional real-time in vivo magnetic paricle imaging," in *Physics in Medicine and Biology*, vol. 54, no. 5, pp. 1-10, 2009.

[34] M. W. Spong, S. Hutchinson, and M. Vidyasagar. "Robot modeling and control," Wiley, 5^{th} edition, December 2006.

[35] I. S. M. Khalil, E. Globovic, and Asif Sabanovic, "High Precision Motion Control of Parallel Robots with Imperfections and Manufacturing Tolerances," in *Proceedings of the IEEE International Conference on Mechatronics*, pp. 39-44, 2011.

[36] K. B. Yesin, K. Vollmers and B. J. Nelson, "Modeling and control of untethered biomicrorobots in a fluidic environment using electromagnetic fields," *International Journal of Robotics Research*, vol. 28, no. 5-6, pp. 527-536, 2006.